HHS Public Access

Author manuscript

Cell Rep. Author manuscript; available in PMC 2021 May 25.

Published in final edited form as:

Cell Rep. 2021 May 04; 35(5): 109071. doi:10.1016/j.celrep.2021.109071.

Pharmacological Wnt ligand inhibition overcomes key tumor-mediated resistance pathways to anti-PD-1 immunotherapy

Nicholas C. DeVito[1], **Michael Sturdivant**[1], **Balamayooran Thievanthiran**[1], **Christine Xiao**[1], **Michael P. Plebanek**[1], **April K.S. Salama**[1], **Georgia M. Beasley**[2], **Alisha Holtzhausen**[3], **Veronica Novotny-Diermayr**[4], **John H. Strickler**[1], **Brent A. Hanks**[1,5,6,*]

[1]Department of Medicine, Division of Medical Oncology, Duke University Medical Center, Duke Cancer Institute, Durham, NC 27710, USA

[2]Department of Surgery, Division of Surgical Oncology, Duke University Medical Center, Duke Cancer Institute, Durham, NC 27710, USA

[3]Lineberger Comprehensive Cancer Center, University of North Carolina at Chapel Hill, Chapel Hill, NC 27599, USA

[4]Experimental Drug Development Centre (EDDC), A*STAR, 10 Biopolis Road, #05-01 Chromos, Singapore 138670, Singapore

[5]Department of Pharmacology and Cancer Biology, Duke University, Durham, NC 27708, USA

[6]Lead contact

SUMMARY

While immune checkpoint blockade is associated with prolonged responses in multiple cancers, most patients still do not benefit from this therapeutic strategy. The Wnt-β-catenin pathway is associated with diminished T cell infiltration; however, activating mutations are rare, implicating a role for autocrine/paracrine Wnt ligand-driven signaling in immune evasion. In this study, we show that proximal mediators of the Wnt signaling pathway are associated with anti-PD-1 resistance, and pharmacologic inhibition of Wnt ligand signaling supports anti-PD-1 efficacy by reversing dendritic cell tolerization and the recruitment of granulocytic myeloid-derived suppressor cells in autochthonous tumor models. We further demonstrate that the inhibition of Wnt signaling promotes the development of a tumor microenvironment that is more conducive to favorable responses to checkpoint blockade in cancer patients. These findings support a rationale for Wnt ligand-focused treatment approaches in future immunotherapy clinical trials and suggest a strategy for selecting those tumors more responsive to Wnt inhibition.

*Correspondence: brent.hanks@duke.edu.

AUTHOR CONTRIBUTIONS

B.A.H., A.H., and J.H.S. conceptualized the project. B.A.H. and N.C.D. designed all experiments. B.A.H., N.C.D., and M.S. analyzed all data. M.S. and C.X. provided technical support. A.K.S.S., G.M.B., and V.N.-D. provided clinical resources for the project. B.A.H. and N.C.D. supervised all experiments. B.A.H., N.C.D., and M.S. wrote the manuscript. B.A.H., N.C.D., A.H., M.S., and M.P.P. reviewed and edited the manuscript.

SUPPLEMENTAL INFORMATION

Supplemental information can be found online at https://doi.org/10.1016/j.celrep.2021.109071.

Graphical abstract

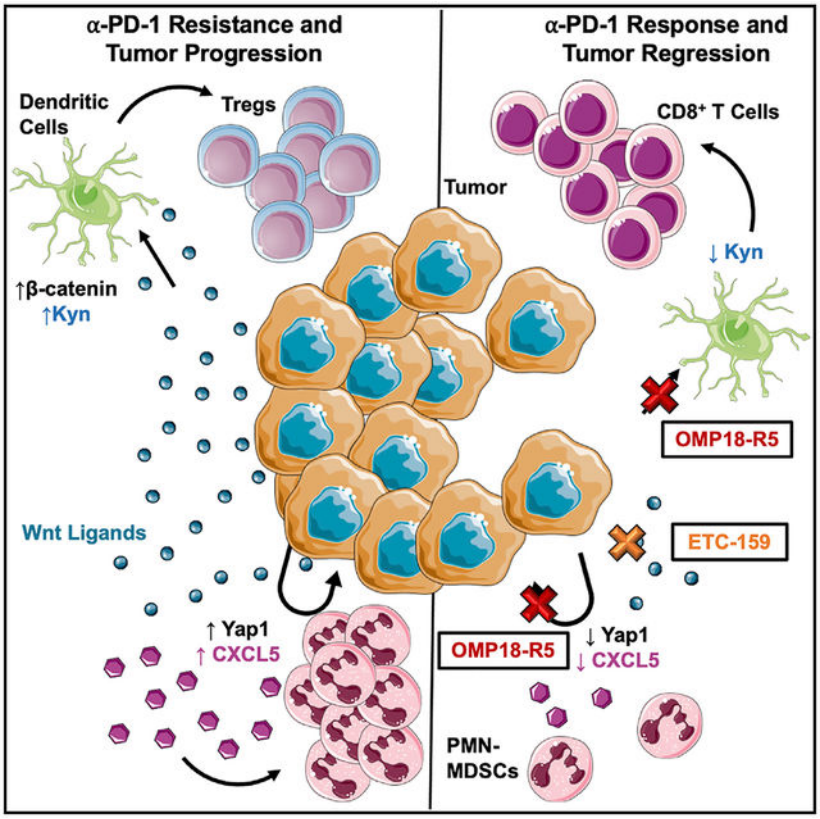

In brief

Anti-PD-1-refractory melanoma exhibits elevated Wnt ligand signaling activity. DeVito et al. demonstrate that pharmacologic inhibition of proximal Wnt ligand signaling sensitizes transgenic models of melanoma and lung cancer to anti-PD-1 checkpoint inhibitor immunotherapy by reversing dendritic cell tolerization and suppressing recruitment of granulocytic myeloid-derived suppressor cells to the tumor bed.

INTRODUCTION

While immune checkpoint inhibitors (ICIs) have demonstrated remarkable responses in metastatic melanoma and non-small cell lung cancer (NSCLC), most of these patients do not respond (Garon et al., 2015; Robert et al., 2015). Moreover, tumors adapt under immunotherapeutic pressure in a subset of responding patients, leading to immune escape and acquired resistance (Gide et al., 2018; Schoenfeld and Hellmann, 2020; Sharma et al., 2017). After initial clinical trial results of the anti-CTLA-4 and anti-PD-1 (aPD1) antibody combination regimen led to its use in selected cancers, other combinations with ICI have largely failed (Gide et al., 2018; Long et al., 2019; Patel and Minn, 2018). These results underscore the importance of a more sophisticated understanding of the interplay between tumor cells and the immune microenvironment that contributes to ICI resistance.

Immune exclusion has been correlated with Wnt/β-catenin pathway activation across multiple tumor types, although mutations in this pathway are rare (Luke et al., 2019; Spranger et al., 2015). This suggests that alterations in Wnt ligands, their endogenous inhibitors, as well as their receptors are likely playing an important role in driving immune evasion. Indeed, our laboratory and those of others have found that Wnt ligands, namely tumor-derived Wnt5a, attenuate the response to aPD1 therapy in mouse models and in patients with metastatic melanoma (Hugo et al., 2016; Zhao et al., 2018b). Wnt5a signals via β-catenin in tumor-associated dendritic cells (DCs), resulting in induction of indoleamine 2,3-dioxygenase (IDO1) activity, enhanced tryptophan (Trp) degradation into kynurenine (Kyn), and the generation of regulatory T cells (Tregs) (Holtzhausen et al., 2015; Zhao et al., 2018b). FoxP3$^+$CD4$^+$ Tregs are frequently present across cancer types and suppress anti-tumor CD8$^+$ T cell responses to circumvent ICI efficacy (Chaudhary and Elkord, 2016; Simpson et al., 2013). Therefore, tumor-induced paracrine Wnt/β-catenin signaling promotes a program of DC tolerogenesis defined by enhanced Treg development and impaired effector T cell priming. Given the crucial role of DCs in ICI activity (Garris et al., 2018; Salmon et al., 2016; Sánchez-Paulete et al., 2016), DC tolerization as a critical ICI resistance mechanism suggests a potential strategy for the development of rational therapeutic combinations (Suryawanshi et al., 2020).

Tumors manipulate the immune microenvironment by recruiting a myriad of cell types that assist in niche formation, metastatic progression, and therapeutic resistance. This includes myeloid-derived suppressor cells (MDSCs), which are a heterogeneous population of myeloid cells that inhibit effector CD8$^+$ T cell activity and have been associated with impaired ICI responses (Marvel and Gabrilovich, 2015; Sade-Feldman et al., 2016; Weber et al., 2016; Weber et al., 2018). Granulocytic MDSCs (polymorphonuclear [PMN]-MDSCs) are recruited to the tumor bed through the expression of CXCR2 ligands, including CXCL2 and CXCL5 (Forsthuber et al., 2019; Highfill et al., 2014; Steele et al., 2016). Our group has found that Wnt5a promotes chemokine-driven recruitment of PMN-MDSCs through autocrine Yap signaling in the tumor, resulting in the suppression of infiltrating activated CD8$^+$ T cells, disease progression, and aPD1 resistance (Theivanthiran et al., 2020). Altogether, these studies implicate tumor-derived Wnt ligand signaling in a broad reprogramming of the immune microenvironment and as a node for both intrinsic and adaptive resistance to immunotherapy. Given these findings, we sought to evaluate the efficacy of several Wnt ligand inhibition strategies in the context of ICI therapy.

Inhibition of the Wnt/β-catenin pathway to date has involved either enhancing β-catenin degradation or blocking its interaction with target genes, impeding the release of Wnt ligands through inhibition of porcupine (PORCN), or by interfering with Wnt ligand-Frizzled (Fzd) receptor binding (Jung and Park, 2020). Given the lack of activating β-catenin pathway mutations, we focused on more proximal pharmacologic approaches that targeted Wnt ligands and their receptors. OMP-18R5 (vantictumab) is a monoclonal antibody (mAb) that binds to Fzd receptors 1, 2, 5, 7, and 8, which has demonstrated safety in phase I studies (Davis et al., 2020). OMP-54F28 (ipafricept), a recombinant fusion protein of Fzd8 and the immunoglobulin (Ig)G1 Fc domain, also interferes with Wnt ligand signaling by acting as an extracellular trap and has proven safety in phase I trials (Moore et al., 2019). Other strategies involve the blockade of PORCN, which catalyzes the palmitoylation of Wnt proteins, which

is necessary for both their secretion as well as their binding to Fzd receptors (Figure 1A). There are several ongoing trials in various combinations with small-molecule PORCN inhibitors including LGK974 (WNT974), RXC004, CGX1321, and ETC-159 (ETC-1922159) (Zhong et al., 2019). Studies to date, however, have focused on targeting tumor-dependent Wnt/β-catenin signaling for chemotherapy resistance rather than modulation of the tumor immune response (Jung and Park, 2020).

Using autochthonous mouse models to better recapitulate the immune tolerization mechanisms observed in human cancers, we characterize the anti-tumor activity and immunological impact of Wnt ligand inhibition in combination with aPD1 in melanoma and NSCLC. This work describes the underlying immunologic mechanisms of these agents within the tumor microenvironment and compares their efficacy with selective IDO1 inhibition. In addition, we explore how the expression of components of the Wnt ligand/Fzd receptor signaling axis correlates with ICI resistance in human melanoma, and we further analyze the immunologic impact of Wnt ligand inhibition in cancer patients.

RESULTS

Wnt ligand signaling influences responses to checkpoint inhibitor therapy

Prior studies have shown an association between Wnt-β-catenin activation and T cell exclusion; however, only ~15% of T cell-poor tumors harbor genetic mutations or copy number variations impacting downstream mediators that drive the activation of the β-catenin signaling pathway (Luke et al., 2019; Spranger et al., 2015). This suggests that paracrine and autocrine Wnt signaling plays an important role in suppressing anti-tumor immunity (Figure 1A). This is consistent with transcriptional analyses demonstrating that escape from aPD1 immunotherapy in an autochthonous model of $BRAF^{V600E}PTEN^{-/-}$(BP) melanoma is associated with enhanced Wnt pathway activation, including elevated expression of several Wnt ligands, Wnt receptors, as well as both canonical and non-canonical targets (Figure 1B).

To examine the role of paracrine and autocrine Wnt ligand signaling in aPD1 resistance in melanoma patients, we first reanalyzed a previously published RNA sequencing (RNA-seq) dataset of patients with metastatic melanoma who had undergone treatment with aPD1 (GEO: GSE78220) (Hugo et al., 2016). This work revealed several Wnt ligands and Fzd receptors to be upregulated in non-responders relative to responders, while the RNF43 E3 ubiquitin ligase, a negative regulator of surface Fzd receptor expression, was reciprocally upregulated in responders (Figure 1C; Table S1). To expand on this analysis, we used a NanoString-based approach to explore the differential expression of Wnt signaling components in aPD1 responding versus non-responding melanoma patients. These data confirmed evidence that both canonical and non-canonical Wnt signaling is elevated in aPD1-refractory melanomas (Figure 1D; Table S2). In addition to an upregulation of Fzd receptors, Wnt ligands, and the co-receptor *LRP5*, expression of both *PYGO1* and *DVL1*, which are known to potentiate Wnt signaling, were also more prominent in non-responding patients (Clevers and Nusse, 2012; Katoh and Katoh, 2007; Mieszczanek et al., 2008) (Figures 1A and 1D). We also observed a significant elevation in *DKK2* and *SFRP2*, which are positively upregulated by the Wnt signaling pathway (Lescher et al., 1998; Li et al., 2005; Xiao et al., 2018). Overall, these data provide supportive evidence that tumors from

aPD1 non-responders exhibit enhanced Wnt signaling activity. Notably, this work further showed an expected increase in *CD8A*, *GZMB*, and *IDO1* expression in aPD1 responders. *IDO1* has been previously described to be upregulated in responders to ICI therapy, likely in response to interferon (IFN)-γ signaling (Gide et al., 2018; Hamid et al., 2011; Yoshida et al., 1981). Importantly, these results in human melanoma are consistent with the murine transcriptional data, highlighting the translatability of the autochthonous BP melanoma model for further studies.

Wnt ligand inhibition suppresses DC-mediated Treg generation

Given recent studies identifying the DC as a critical mediator of immunologic responses to aPD1 (Salmon et al., 2016; Spranger et al., 2017), and our previous data implicating Wnt5a in DC-mediated Treg differentiation (Holtzhausen et al., 2015; Zhao et al., 2018b), we set out to develop a pharmacologic strategy to reverse Wnt ligand-mediated DC tolerization (Figure 1A). The Fzd receptor antagonistic antibody OMP-18R5 and the Wnt ligand trap OMP-54F28 both inhibit Wnt ligand induction of β-catenin activation in 293T-TCF/LEF luciferase reporter assays (Figures 2A and S1A) (Fischer et al., 2017; Gurney et al., 2012; Jimeno et al., 2017; Moore et al., 2019). Similarly, these inhibitors suppressed β-catenin levels in transgenic melanomas *in situ* (Figure S1B). Further work showed these agents also inhibit Wnt-induced IDO1 expression by DCs and reverse Wnt5a-induced DC-mediated Treg generation *in vitro* (Figures 2B, 2C, and S1C). This is consistent with our previous studies demonstrating that the PORCN inhibitor, C59, blocks both the secretion of the Wnt5a ligand as well as melanoma-mediated upregulation of IDO1 expression by DCs (Holtzhausen et al., 2015) (Figure 1A). In a similar fashion to OMP-18R5, treatment of a melanoma cell line derived from the autochthonous BP model with C59 reverses tumor conditioned media (CM)-induced DC-dependent Treg generation (Figure 2D).

Wnt ligand inhibition enhances aPD1 therapy in an autochthonous model of melanoma

To further determine the effects of pharmacologic Wnt ligand inhibition *in vivo* and evaluate synergy with aPD1 antibody immunotherapy, we performed additional experiments utilizing the syngeneic BP melanoma model. Both OMP-54F28 and OMP-18R5 in combination with aPD1 were found to suppress primary tumor growth over aPD1 alone (Figure 2E). In addition, Wnt ligand inhibition in combination with aPD1 eliminated metastatic progression to the lung based on hematoxylin and eosin (H&E) staining (Figures 2F and S1D). Further immunohistochemistry (IHC) studies showed that both Wnt ligand inhibitors enhanced tumor $CD8^+$ T cell infiltration, although OMP-18R5 generated the most robust anti-tumor immune response (Figures 2G and S1E). This is consistent with an increase in the tumor-infiltrating $CD8^+$ T cell/Treg ratio following OMP-18R5/aPD1 combination therapy based on flow cytometry (Figure 2H).

We have previously demonstrated that the autochthonous BP melanoma model exhibits a modest response to aPD1 immunotherapy followed by disease progression despite continued PD-1 blockade (Zhao et al., 2018a). In this model, combination OMP-18R5/aPD1 effectively impedes primary melanoma progression compared to aPD1 alone, while additional H&E studies also demonstrated a suppression in lung metastasis (Figures 3A, 3B, and S2A). Importantly, this anti-tumor effect correlated with enhanced tumor-infiltrating

$CD8^+$ T cell/Treg ratios as well as increased numbers of infiltrating $CD8^+$ T cells specific to the melanoma-associated antigen, tyrosinase-related protein-2 (TRP2), based on IFN-γ enzyme-linked immunospot (ELISpot) assays (Figures 3C, 3D, S2B, and S2C). A more modest anti-tumor immune effect was observed in the same tumor model with OMP-54F28 (Figure S3), which led us to primarily pursue the analysis of OMP-18R5 in subsequent experiments.

The concept of pharmacologic Wnt signaling inhibition was initially developed to limit stem cell longevity and therefore inhibit tumor progression (Krishnamurthy and Kurzrock, 2018). To determine whether Wnt inhibition impacted tumor cell proliferation in our model, we conducted *in vitro* studies showing that neither OMP-18R5 nor OMP-54F28 affected BP melanoma cell proliferation (Figure S2D). To further investigate whether the effects of Wnt ligand inhibition in the BP transgenic melanoma model is dependent on the host immune system, we repeated the above *in vivo* experiment following antibody-directed ablation of $CD8^+$ T cells (Figure S2E). Importantly, this study demonstrated that the ablation of effector $CD8^+$ T cells eliminated the therapeutic effect of OMP-18R5, indicating that Wnt inhibition suppresses primary and metastatic progression via a cytotoxic T cell-mediated mechanism (Figures 3E, S2E, and S2F).

Our previous data suggest that aPD1-refractory melanomas may be more sensitive to Wnt ligand inhibition (Figures 1B–1D). To test this hypothesis, we repeated the above experiment in the BP transgenic melanoma model but delayed the introduction of a small molecule PORCN inhibitor, ETC-159, to block Wnt ligand secretion until approximately day 14 of treatment with aPD1, allowing sufficient time for the development of ICI resistance (Zhao et al., 2018a). Consistent with our prior observations that aPD1 resistance is associated with enhanced Wnt ligand signaling (Figures 1B–1D), the introduction of the ETC-159 PORCN inhibitor stabilized primary tumor progression in the autochthonous melanoma model (Figure 3F). These effects correlated with a significant increase in tumor-infiltrating $CD8^+$ T cells and a diminished number of tumor-resident Tregs (Figure 3G). We also observed ETC-159 to correspondingly inhibit the enhanced β-catenin signaling observed during aPD1 therapy in tumor-associated DC populations (Figure 3H) as well as in the tumor tissues themselves (Figure 3I). Overall, these studies suggest that Wnt ligand inhibition augments aPD1 efficacy in a manner at least partially dependent on the host immune system.

Wnt ligand inhibition enhances aPD1 therapy in an autochthonous model of NSCLC

To determine whether the immunologic impact of Wnt inhibition exists beyond melanoma, we turned our attention toward additional studies focused on NSCLC. Relative to melanoma, the response rates to aPD1 in NSCLC patients have been more modest (Reck et al., 2016). As a result, there is an urgent need for strategies to enhance the efficacy of ICI therapy in NSCLC. Initially, we performed a similarly designed experiment using the syngeneic Lewis lung carcinoma (LLC) model. We observed OMP-18R5/aPD1 combination therapy to modestly suppress primary tumor progression while significantly enhancing numbers of tumor-infiltrating $CD8^+$ T cells, including an increased population of $CD8^+$ T cells capable of recognizing the LLC-associated tumor antigen MUT1 (Figures S4A–S4C) (Mandelboim et al., 1994).

To test whether these effects could further extend to an autochthonous model of NSCLC, we initiated studies using the $Kras^{G12D}p53^{flox/flox}$ (KP) NSCLC system that can be induced via the intra-nasal delivery of a Cre recombinase-expressing adenovirus (Ad-Cre) (DuPage et al., 2009). Since tumors from these mice have been shown to contain a Wnt-producing niche, we hypothesized that Wnt ligands could be driving a similar aPD1 resistance program as in melanoma (Tammela et al., 2017). Approximately 8–10 weeks following Ad-Cre delivery, mice underwent baseline micro-computed tomography (micro-CT) imaging followed by therapy. Serial micro-CT imaging and tumor volume contouring were utilized at weeks 14 and 17 to monitor primary tumor progression in the lung in each treatment group. This work demonstrated the OMP-18R5/aPD1 combination regimen to be superior to aPD1 mAb monotherapy (Figures 4A, 4B, S4D, and S4E). This imaging data correlated well with diminished lung weights in the OMP-18R5/aPD1 combination group and was further supported by a reduced pulmonary tumor burden based on H&E microscopy (Figures 4C and 4D). Anti-tumor responses to the OMP-18R5/aPD1 combination regimen further correlated with enhanced $CD8^+$ T cell infiltration into tumor tissues as well as with the development of enhanced numbers of tumor antigen-specific $CD8^+$ T cells (Figures 4E, 4F, S4F, and S4G). Importantly, all of these findings were in line with improved survival of the KP mice in the combination treatment group over aPD1 monotherapy (Figure 4G). These data further indicate that Wnt ligand inhibition promotes the generation of an effective anti-tumor immune response in multiple tumor histologies and supports the therapeutic relevance of targeting Wnt ligand signaling.

Wnt ligand inhibition diminishes local Kyn levels in the tumor microenvironment

The immunoregulatory enzyme IDO1 has been shown to play an important role in regulating anti-tumor immunity by suppressing effector $CD8^+$ T cell expansion while driving Treg differentiation through the production of the metabolite Kyn (Munn and Mellor, 2007; Munn and Mellor, 2016). While extensive literature has described the critical role of IDO1 in the regulation of anti-tumor immunity in both pre-clinical and early clinical studies, a recent phase III clinical trial (KEYNOTE-252/ECHO-301) showed that the selective IDO1 inhibitor epacadostat in combination with pembrolizumab failed to improve clinical outcomes for metastatic melanoma patients relative to pembrolizumab alone (Long et al., 2019). These disappointing results have been hypothesized to be due, at least in part, to compensatory Trp degrading enzymes that also contribute to Kyn levels such as TDO2 (Muller et al., 2019). We have previously demonstrated that Wnt5a ligand signaling in local DC populations within the tumor microenvironment drives the expression of IDO1 (Holtzhausen et al., 2015). Further studies have shown this same Wnt-dependent pathway to promote the synthesis of protoporphyrin IX (PpIX), a heme-derived compound, which serves as the rate-limiting prosthetic group for both IDO1 and TDO2 (Lewis-Ballester et al., 2016; Zhao et al., 2018b). Based on these data, we hypothesized that the inhibition of paracrine Wnt ligand signaling could result in potent suppression of Kyn production by DCs in the tumor and lymph node (LN) microenvironments (Metz et al., 2010) (Figure 5A). Initial studies found that Wnt ligand blockade suppresses the synthesis of PpIX in DCs by flow cytometry (Zhao et al., 2018b) (Figure 5B). These results demonstrated this pharmacologic strategy to regulate the activity of other Trp degrading enzymes beyond IDO1 in DCs. Notably, we found no evidence that this pathway regulates tumor-dependent

expression of either IDO1 or TDO2 or DC-dependent expression of TDO2 (Figures S5A and S5B). In addition, tumor cell PpIX levels were not impacted by Wnt5a stimulation, suggesting that the Wnt ligand effect on this pathway is restricted to DCs and perhaps other antigen-presenting cells (APCs) in the tumor microenvironment (Figure S5C) (Zhao et al., 2018b).

To test whether Wnt ligand inhibition effectively suppresses Kyn generation and subsequent Treg differentiation *in vivo*, we performed a multi-arm experiment utilizing the autochthonous BP melanoma model to compare the ability of epacadostat versus OMP-18R5 to enhance the efficacy of aPD1. This work demonstrated OMP-18R5 to reproducibly suppress melanoma progression more effectively than epacadostat when combined with aPD1 (Figure 5C). Combination OMP-18R5/aPD1 therapy also enhanced the generation of TRP2-specific $CD8^+$ T cells based on IFN-γ ELISpot analysis compared to epacadostat/aPD1 (Figures 5D and S5D). To determine whether the therapeutic effect observed by OMP-18R5 is associated with its ability to suppress Kyn levels *in situ*, we harvested both tumor and LN tissues from melanoma-bearing mice undergoing treatment with either epacadostat or OMP-18R5 for analysis by a Kyn-specific enzyme-linked immunosorbent assay (ELISA) and liquid chromatography-tandem mass spectrometry (LC-MS/MS). As expected, diminished levels of Kyn were observed in both tumor and tumor-draining LN (TDLN) tissues following treatment with epacadostat, while these levels trended lower in those tissues exposed to OMP-18R5 (Figures 5E, S5E, and S5F). Consistent with these findings, we identified a more substantial suppression in tumor-infiltrating Treg populations following OMP-18R5/aPD1 over epacadostat/aPD1 (Figure 5F). Based on our data suggesting that Wnt signaling activity is enhanced in the aPD1-refractory setting (Figures 1 and 3H), we further postulated that the inhibition of Wnt ligand signaling would be superior to selective IDO1 inhibitor therapy in aPD1-resistant tumors. We therefore compared delayed epacadostat to delayed ETC-159 after prior exposure to aPD1 mAb in the autochthonous BP melanoma model. Indeed, this study also found ETC-159 to impair tumor growth more effectively than epacadostat following progression through continuous aPD1 therapy (Figure 5G).

Altogether, these data suggest that Wnt ligand inhibition enhances anti-tumor immunity at least partially by suppressing the production of Kyn in the tumor and TDLN microenvironment. These studies provide support for pharmacologically targeting the upstream regulatory pathways common to all Trp-degrading enzymes as a strategy for suppressing Kyn generation and Treg development. However, reconciling the relative levels of Kyn following Wnt ligand inhibition versus IDO1 inhibition with the superior anti-tumor response observed with Wnt targeted therapy, we hypothesized that the immunological impact of Wnt inhibition may extend beyond the inhibition of Kyn production. We therefore initiated studies to investigate alternative mechanisms by which Wnt ligand blockade may support responses to checkpoint inhibitor immunotherapy.

Wnt ligand inhibition suppresses PMN-MDSC recruitment to the tumor bed

We have found that a noncanonical Wnt ligand-YAP signaling axis plays an important role in regulating the recruitment of PMN-MDSCs to the tumor bed by promoting the expression

of CXCR2-dependent chemokines in response to PD-1 blockade (Theivanthiran et al., 2020). Notably, this study found the CXCL5 chemokine to be most responsive to aPD1 therapy as well as to Wnt5a stimulation and demonstrated the recruitment of this PMN-MDSC population to suppress $CD8^+$ T cell responses and promote tumor progression. We therefore hypothesized that Wnt ligand inhibition would inhibit CXCL5 chemokine expression and suppress PMN-MDSC accumulation in tumors. Indeed, we found OMP-18R5 to inhibit Wnt5a-dependent CXCL5 expression and YAP1 stabilization by BP melanoma cells *in vitro*, as well as CXCL5 expression by BP melanomas *in vivo* (Figures 6A–6C). Similarly, ETC-159 suppressed aPD1-induced CXCL5 and CXCL2 expression by BP melanomas *in vivo* based on qRT-PCR analysis (Figures 6D and S6A). Consistent with our prior studies, we found that tumor-associated PMN-MDSCs increase in response to aPD1, but this effect diminished with the addition of either ETC-159 or OMP-18R5 (Figures 6E, 6F, and S6B) (Theivanthiran et al., 2020). Furthermore, Wnt inhibitor-mediated suppression of PMN-MDSC recruitment is independent of the tumor model since we observed a similar inhibition of PMN-MDSC recruitment to LLC tumors following OMP-18R5 treatment (Figure 6G).

These data suggest that Wnt ligand inhibition can generate an immune microenvironment that is more conducive to the development of anti-tumor immunity via multiple mechanisms. In light of prior studies highlighting a negative relationship between circulating levels of PMN-MDSCs and the efficacy of aPD1, these data suggest that Wnt ligand inhibition is expected to augment responses to checkpoint inhibitor immunotherapy by also blocking PMN-MDSC recruitment to the tumor bed (Meyer et al., 2014; Weber et al., 2016).

Wnt ligand inhibition promotes the development of an immune microenvironment that is more conducive to checkpoint inhibitor responses in cancer patients

During a phase I all-solid tumor dose-escalation study conducted with the ETC-159 PORCN inhibitor, a patient with colorectal cancer (CRC) with RSPO fusion (patient #1) and a patient with presumed cholangiocarcinoma (patient #2) each underwent both pre- and post-treatment tissue biopsies, allowing for differential gene expression studies using the NanoString transcriptional analysis platform (Figure 7A; Table S3). Overlapping increases in several genes associated with enhanced immunogenicity, including *CD8A*, *CD27*, *CD40*, *IFNG*, *PDCD1* (PD-1), and various granzyme isoforms were observed in both patients as well as *CD86* and *PRF1* in patient #2. In addition, multiple genes associated with immunosuppression, including *ARG1* and *ARG2*, the MDSC recruiting chemokines *CXCL1/CXCL2* and *IL10*, and the Treg markers *FOXP3* and *NRP1* (neuropilin) were downregulated with ETC-159 treatment (Figure 7B; Table S4). Finally, both treated tumors exhibited decreased TCF7 and CCND3 expression, verifying downstream inhibition of the Wnt/β-catenin pathway (Figure S6C).

Overall, these results support our pre-clinical data and indicate that Wnt ligand blockade represents a promising strategy for converting the tumor microenvironment into a more favorable state for the generation of an effective anti-tumor immune response to aPD1.

Wnt ligand inhibition does not significantly impact tumor DC recruitment

Previous studies have shown that stabilization (STA) of β-catenin in a related $BRAF^{V600E}PTEN^{-/-}Bcat^{STA}$ melanoma model suppresses tumor CCL4 expression, reducing antigen cross-presenting $CD103^{+}$major histocompatibility complex class II (MHC class II)$^{+}CD11c^{+}$ DC recruitment and ultimately suppressing tumor T cell infiltration (Damsky et al., 2011; Spranger et al., 2015). While we observed a modest increase in the expression of DC-associated genes, *ITGAX* and *FLT3L*, in response to Wnt ligand inhibition in patient #1 (Figure 7B; Table S4), these changes were not observed in patient #2 despite a significant increase in cytolytic T cell markers in the treated tumor. Moreover, we did not appreciate an increase in the tumor-infiltrating $CD103^{+}$ subset of MHC class II $^{+}CD11c^{+}$ DCs with combination aPD1 and OMP-18R5 (Figure S7A, left) or ETC-159 in the BP melanoma model (Figure S7A, right). We also did not see meaningful alterations in *Ccl4* expression in murine tumors treated with OMP-18R5 or ETC-159 and did not observe differences in *CCL4* or *ATF3* expression levels between aPD1 responder and non-responder melanoma patients in the Hugo et al. (2016) human RNA-seq dataset (Figures S7B and S7C). Larger tissue-based studies will be necessary to determine the relative role of DC recruitment on the observed immunological impact of pharmacologic Wnt pathway inhibition.

DISCUSSION

The Wnt/β-catenin signaling pathway has been associated with tumor immune evasion as well as ICI resistance in mouse models and patients (Holtzhausen et al., 2015; Luke et al., 2019; Spranger et al., 2015; Theivanthiran et al., 2020). Research thus far suggests that this process occurs through at least three mechanisms: paracrine Wnt ligand-induced DC tolerance (Holtzhausen et al., 2015; Hong et al., 2015a; Manicassamy et al., 2010; Zhao et al., 2018b), autocrine Wnt ligand-driven PMN-MDSC recruitment (Theivanthiran et al., 2020), and tumor-intrinsic β-catenin signaling, leading to a suppression of CCL4 and a reduction in the influx of $CD103^{+}$ antigen cross-presenting DCs into the tumor bed (Spranger et al., 2015).

The observation that only a limited percentage of T cell-poor tumors harbor downstream activating mutations that drive the β-catenin signaling pathway strongly suggests that regulators of paracrine and autocrine Wnt ligand activity contribute to immune exclusion (Luke et al., 2019; Spranger et al., 2015). Indeed, mutations promoting activation of the Wnt/β-catenin pathway in CRCs are not associated with differences in immune cell infiltration, further supporting this concept (Mlecnik et al., 2016). Additionally, our previous data indicate that a non-canonical YAP-dependent pathway in tumors is responsible for promoting PMN-MDSC recruitment in response to Wnt5a, implying that alterations impacting upstream paracrine/autocrine Wnt ligand signaling are likely to play an important role beyond downstream mutations exclusively activating the canonical Wnt/β-catenin signaling pathway. This is consistent with our finding of increased expression levels of *SFRP2* in aPD1-resistant melanomas, which has been shown to promote a shift toward non-canonical pathway activation (Brinkmann et al., 2016; Sun et al., 2016). These findings led

us to investigate whether modulating upstream paracrine/autocrine Wnt ligand signaling could influence aPD1 outcomes.

We observed that pharmacologic inhibition of Wnt ligand-receptor interactions enhanced aPD1 in both syngeneic and autochthonous models of melanoma. This was attributable to the effect of Wnt ligand inhibition on the immune system, as this strategy does not affect tumor cell proliferation *in vitro* and requires $CD8^+$ T cells for activity *in vivo*. This is further supported by studies showing Wnt ligand inhibition to promote tumor antigen-specific $CD8^+$ T cell responses while reducing tumor-infiltrating Treg and PMN-MDSC populations within tumors. Indeed, this is also consistent with our finding that treatment of cancer patients with ETC-159 alters the tumor immune microenvironment in a manner that is expected to be more favorable for generating responses to checkpoint inhibitor therapy.

To further investigate activity outside of melanoma, we also examined the immunologic impact of Wnt ligand inhibition in a LLC model and a KP autochthonous model of NSCLC. Initial studies showed Wnt ligand inhibition to sensitize LLC tumors to ICI therapy. Contrary to previous observations showing a lack of response to dual immune checkpoint blockade in the autochthonous NSCLC model (Pfirschke et al., 2016), additional studies demonstrated that Wnt ligand inhibitor/aPD1 combination therapy enhanced tumor antigen-specific immunity while suppressing tumor progression and extending survival. Overall, we demonstrate that Wnt ligand inhibition improves aPD1 responses in two clinically relevant autochthonous mouse models of melanoma and NSCLC.

DCs direct the cellular cytotoxic immune response and are necessary for successful immune checkpoint blockade (Garris et al., 2018). Previously, we associated the Wnt/β-catenin cascade with DC tolerance through induction of IDO1 expression and enzymatic activity, culminating in Treg generation via Kyn production (Zhao et al., 2018b). In the present study, we found that Wnt ligand inhibition reversed β-catenin signaling in tumor-draining LN DCs while inhibiting tryptophan-degrading enzymatic activity both *in vitro* and *in vivo*. These data were consistent with the additional finding that Wnt ligand inhibition suppressed DC PpIX synthesis (Zhao et al., 2018b). While DC-mediated Treg generation was induced by Wnt ligand stimulation or tumor-conditioned media, as we have observed previously (Holtzhausen et al., 2015), this effect could be reversed by Fzd receptor blockade and PORCN inhibition, respectively. These results are consistent with data generated by others showing that targeting the Wnt/β-catenin pathway via DC-specific genetic deletion of LRP co-receptors can enhance anti-tumor immunity (Hong et al., 2015b; Manicassamy et al., 2010). These results are further in line with recent studies showing ETC-159 to improve $CD8^+$ T cell/Treg ratios in a humanized mouse model of microsatellite stable CRC (Bagby et al., 2020).

Given that others have demonstrated the Wnt/β-catenin pathway to suppress DC recruitment through CCL4 repression, we evaluated $CD103^+$ DC accumulation in the tumor bed and alterations in CCL4 in the tumor microenvironment in response to Wnt ligand inhibition. We did not observe significant differences by either of these parameters to sufficiently account for the mechanism of action of Wnt inhibition (Figure S7). Opposed to our studies that used a BP autochthonous melanoma model treated with pharmacologic inhibitors to the Wnt

ligand signaling pathway, Spranger et al. (2015) utilized a constitutively active β-catenin derivative of the BP melanoma model. The discrepancies in these results may be associated with the relative differences in potency between genetic activation and the pharmacologic inhibition of the β-catenin pathway. However, the differential impact of these models on non-canonical Wnt signaling may also be a contributing factor.

Significant scientific effort has been invested in developing methods of inhibiting Trp catabolizing enzymes (Hou et al., 2007; Muller et al., 2005; Munn, 2012). The selective IDO1 inhibitor epacadostat showed promise in preclinical studies (Prendergast et al., 2017); however, it did not achieve any meaningful activity in a recent phase III clinical trial at the selected dose (Long et al., 2019). Our data indicate that targeting Wnt ligands, which are upstream regulators of IDO1 and TDO2 activity, can outperform selective IDO1 inhibition in the generation of antigen-specific T cell responses as well as the control of primary tumor growth at least, in part, by suppressing Kyn production and Treg differentiation. In addition to supporting the immunologic significance of blocking Wnt ligand signaling, these data further suggest that a Wnt ligand genetic signature may serve as a predictive biomarker for targeted IDO1/TDO2 inhibitors (Holtzhausen et al., 2015). A previous study has shown that tumor-expressed IDO1 promotes the recruitment of MDSCs via Tregs using an IDO1-overexpressing B16 model (Holmgaard et al., 2015). We did not find differences in intratumoral MDSCs with epacadostat treatment in our system. Moreover, our results and previously published observations (Theivanthiran et al., 2020) point toward an autocrine Wnt ligand-induced upregulation of PMN-MDSC recruiting chemokines. This is further supported by our observations that OMP-18R5 impairs Wnt ligand-induced CXCL5 production in our melanoma cell line *in vitro* and the autochthonous melanoma model *in vivo*. We have thus expanded upon our previous findings where autocrine tumor Wnt ligand stimulation supports PMN-MDSC recruitment during aPD1 treatment by demonstrating that this process is reversible with various Wnt ligand inhibition strategies. Notably, we have not observed any alterations in monocyte or macro-phage populations with Wnt ligand inhibitors, suggesting that the effect of Wnt ligand inhibition may be restricted to PMN-MDSCs. While others have observed Wnt pathway activation in association with resistance to immunotherapy, a higher resolution analysis of the Wnt ligand/Fzd receptor signaling axis as a driver of aPD1 resistance has not previously been conducted (Gide et al., 2018).

A relevant concern associated with targeting the Wnt/β-catenin pathway clinically is adverse effects (AEs), which could hinder treatment efficacy and feasibility, particularly in combination with other agents. A phase I study of patients treated with single-agent PORCN inhibitor LGK974 (WNT974) showed grade 3/4 AEs including asthenia and fatigue in 2% of patients (Janku et al., 2015). Phase I data on OMP-18R5 reported grade 3/4 drug-related AEs, including nausea, fatigue, and dysgeusia in 29% of patients, while OMP-54F28 has been associated with grade 3 AEs, including neutropenia in 21.6% of patients (Davis et al., 2020; Moore et al., 2019). Bone-related AEs, including bone fracture, emerged in the initial part of both phase I studies and were not observed subsequently after monitoring protocols, intermittent dosing, and prophylactic bone protective agents were initiated (Davis et al., 2020; Moore et al., 2019). This safety profile has been manageable and lacks immune-related AEs, an encouraging attribute for combining these agents with ICI therapy (Janku et al., 2020).

This current study has important limitations to be considered. Fzd receptor blockade may differ in its mechanism of action from the ablation of all soluble Wnt ligands. Although we did not compare OMP-18R5 directly to ETC-159, the *in vitro* and *in vivo* activities associated with these agents were consistently similar. Given our previous data, we did not extensively examine the potential effects of Wnt inhibition on cell types other than tumor cells, PMN-MDSCs, and DCs. Further investigation is warranted into the effect that this treatment strategy may have on the diverse tumor microenvironment, particularly in patients as Wnt inhibition progresses into clinical trials with ICI therapies. Finally, the clinical specimen-derived data presented herein are based on a limited number of samples. Additional correlative studies are needed to expand these studies to a larger array of tumor types in a larger cohort of patients.

In summary, we demonstrate that Wnt ligand inhibition enhances aPD1 therapy and rescues tumors progressing through aPD1 in autochthonous mouse models that recapitulate human melanoma and NSCLC. By attenuating tumor-induced DC tolerance and PMN-MDSC recruitment, inhibiting Wnt ligand signaling affects critical nodes in tumor immune escape and addresses key drivers of immunotherapy resistance. We further provide correlative data derived from clinical tumor specimens, indicating that Wnt ligand inhibition can support cytolytic T cell activity in human tumors. PORCN inhibitors, including ETC-159, are currently being investigated in combination with aPD1 mAb therapies in early phase clinical trials. Our preclinical and correlative clinical data can inform treatment sequencing as well as biomarker development for future trials investigating this strategy. Importantly, these data suggest that tumors exhibiting elevated levels of paracrine/autocrine Wnt signaling activity based on gene expression profiling studies would be expected to respond more favorably to combination aPD1/Wnt ligand inhibitor therapy over aPD1 monotherapy. Cumulatively, our work demonstrates that pharmacologic inhibition of Wnt ligands represents a promising approach for reversing tumor-mediated immune tolerance and enhancing the efficacy of PD-1 blockade.

STAR★METHODS

RESOURCE AVAILABILITY

Lead contact—Further information and requests for resources and reagents should be directed to and will be fulfilled by the Lead Contact Brent A. Hanks, M.D., Ph.D. (brent.hanks@duke.edu).

Materials availability—This study did not generate new unique reagents.

Data and code availability—RNA-seq data derived from the BP melanoma anti-PD-1 resistance study is available on the Sequence Read Archive (SRA) database, accession number SAMN09878780 (Theivanthiran et al., 2020; Zhao et al., 2018a). RNA-seq data derived from the Hugo et al. human melanoma anti-PD-1 resistance study was originally deposited onto the GEO Database under accession number, GEO: GSE78220 (Hugo et al., 2016). Nanostring data from metastatic melanoma patient samples prior to anti-PD-1 and from patients treated with ETC-159 were deposited to the GEO Database under the accession numbers GEO: GSE165745 and GSE167039, respectively.

EXPERIMENTAL MODEL AND SUBJECT DETAILS

Autochthonous and syngeneic mouse studies—Mouse experiments were performed in accordance with a protocol approved by the Institutional Animal Care and Use Committee (IACUC) of Duke University Medical Center. B6.CgBRAF^{tm1Mmcm}PTEN^{tm1Hwu}Tg(TyrCre/ERT2)13Bos/BosJ (BRAF^{V600E} PTEN$^{-/-}$, BP, H-2^{b}) transgenic mice (Jackson Labs, IMSR Cat# JAX:013590, RRID:IMSR_JAX:013590) were sub-dermally injected with 4-HT (38.75 μg/mouse; Sigma-Aldrich, H6278–10MG) to induce primary melanoma development at the base of the tail. BP melanoma and Lewis lung carcinoma cell lines were implanted by subcutaneous injection at the base of the tail of syngeneic C57BL/6J mice (Jackson Labs, IMSR Cat# JAX_000664, RRID:IMSR_JAX:000664). Tumor bearing mice were randomized into treatment groups when tumors reached approximately 65–100 mm^3 (0.065–0.1 cm^3). Tumor volumes were calculated according to the following formulas:

$$\text{cm}^3 = \left[(\text{length,cm}) \times (\text{width,cm})^2\right] \div 2$$

$$\text{mm}^3 = \left[(\text{length,mm}) \times (\text{width,mm})^2\right] \div 2$$

All experimental groups included randomly chosen littermates of both sexes, ages 6–8 weeks, and of the same strain. Melanoma and LLC growth was monitored by orthogonal caliper measurements every 3–4 days. Normalized tumor volumes were used to display data related to the autochthonous melanoma model to account for variations in primary tumor size. Kras^{G12D}p53$^{flox/flox}$ (KP) mice (a gift from Anton Berns, the Netherlands Cancer Institute) were anesthetized with isoflurane and administered Ad5CMVCre (University of Iowa) adenovirus vector intra-nasally to induce lung adenocarcinoma development (DuPage et al., 2009). Mice ages 6–8 weeks and littermates of both sexes were randomly assigned to treatment cohorts 10 weeks after virus administration. These mice were monitored by micro-CT imaging as described below. Mice were treated with rat IgG2a isotype control (BioXCell, BE0089) or anti-PD-1 mAb at 200 μg/dose (BioXCell, RMP-14, BE0146) every 3 days via intraperitoneal (i.p.) injection. OMP-18R5 and OMP-54F28 (OncoMed) were given weekly via i.p. injection at 400 μg/dose. ETC-159 (A*STAR) in polyethylene glycol (PEG, Sigma-Aldrich, 89510–250G-F) vehicle or PEG alone was given orally at 200 μg/dose every 3 days. CD8 depletion was conducted as previously described (Zhao et al., 2018a). B6.Cg-Foxp3^{tm2Tch}/J (FoxP-EGFP, H-2^{b}) transgenic mice and BALB/c mice (H-2^{d}) were purchased from Jackson Labs (IMSR Cat# JAX_000651,RRID:IMSR_JAX:000651, IMSR Cat# JAX:006772, RRID:IMSR_JAX:006772) for performing Treg differentiation assays. All mice, regardless of experiment and strain were housed in an isolated animal facility requiring personal protective clothing for entry and monitored by Duke veterinary staff. Mice are housed in micro-isolator caging, up to 5 mice per cage, on corn cob bedding and changed every two weeks. Temperature, humidity and pressures of the mouse facility are controlled by a pneumatic control system with digital backup alarms. Exhaust systems and air supply is HEPA filtered. Species-specific heat and humidity are maintained within the parameters outlined in *The Guide for the Care and Use of Laboratory Animals*. All mice

were euthanized by a carbon dioxide (CO2) euthanasia chamber followed by cervical dislocation.

Cell lines—$Braf^{V600E}Pten^{-/-}$(BPD6, male) cell lines were generated and cultured in DMEM with 10% FBS at 37°C as previously described (Holtzhausen et al., 2015). $Kras^{G12D}p53^{flox/flox}$ cell lines were generated through enzymatic and mechanical digestion of autochthonous mouse lungs during week 16 post-virus administration by visual tumor dissection and serial culturing in DMEM with 10% FBS to remove fibroblasts. Cell lines were confirmed by rt-PCR and western blot. Lewis Lung Carcinoma cells were purchased from the ATCC (ATCC, CRL-1642) and cultured according to the supplier's specifications. Bone marrow-derived dendritic cells (BMDCs) were harvested and differentiated using IL-4 (BioAbChem, 42-IL4 C) and GM-CSF (BioAbChem, 42-GMCSF) as previously described and purified using CD11c microbeads (Miltenyi Biotec, 130-108-338) according to the manufacturer's protocol (Inaba et al., 1992). The HEK293-LEF1/TCF-luciferase cell line was cultured in DMEM with 10% FBS as previously described in the presence or absence of OMP-18R5 or OMP-54F28 (Ring et al., 2011). The murine dendritic cell line, DC2.4 (a generous gift from Dr. Kenneth Rock, University of Massachusetts Medical School) was cultured and generated as previously described (Shen et al., 1997).

Human studies—The archival melanoma tissue specimen study associated with this work was approved by the Duke University Medical Center institutional review board (IRB) (ClinicalTrials.gov: NCT02694965). Only treatment naive patients that underwent anti-PD-1 monotherapy with either pembrolizumab (200 mg IV every 3 weeks) or nivolumab (240 mg IV every 2 weeks) were included. All patients provided written consent and archival specimens were selected from available tissues. Patient demographics are provided in Table S2. Patient demographics associated with the tissue specimen studies derived from the Phase I ETC-159 clinical trial (ClinicalTrials.gov: NCT02521844) are described in Table S3.

METHOD DETAILS

Flow cytometry—Tumor tissues were resected and processed using the following tissue digestion mixture: collagenase IV (1 g/100mL HBSS, 10x stock, Sigma-Aldrich, C-5138), hyaluronidase (100 mg/100mL HBSS, 10x stock solution, Sigma-Aldrich, H-6254), DNaseI (20,000 U/100mL HBSS, 10x stock solution, Sigma-Aldrich, D-5025) in serum free RPMI (Sigma-Aldrich, R8758) followed by mechanical dissociation with gentleMACS Tissue Dissociator (Miltenyi Biotec, 130-093-235) using gentleMACSC-tubes (Miltenyi Biotec, 130-093-237) and incubation at 37°C with agitation at 250 rpm for 30 minutes. Single Cell suspension was lysed with red blood cell (RBC) lysis buffer (Sigma-Aldrich, R7757) according to the manufacturer's protocol. One million cells were stained with 1 μg per million cells of each fluorochrome conjugated antibodies or commercially available dyes according to the standard protocols and analyzed using a FACSCanto II or LSRII flow cytometer (Becton Dickinson). The following antibodies were used: Anti-mouse CD45, PerCp-Cy5.5 conjugated, clone:30-F11 (BD PharMingen, 550994). Anti-mouse CD3e, FITC conjugated, clone: 145-2C11 (BD PharMingen, 553061). Anti-mouse CD8a, BV510 conjugated, clone: 53-6.7 (BD PharMingen, 563068). Anti-mouse CD4, APC conjugated, clone: RM4-5 (BD PharMingen, 553051). Anti-mouse Foxp3, PE conjugated, clone: MF23

(BD PharMingen, 560408). Anti-mouse CD11b, PE conjugated, clone: M1/70 (BD PharMingen, 557397). Anti-mouse F4/80, APC conjugated, clone: BM8 (Biolegend, 123116). Anti-mouse Ly-6G, FITC conjugated, clone: 1A8 (BD PharMingen, 551460). Anti-mouse CD16/CD32 (Fc block), clone: 2.4G2(BD PharMingen, 553142). Anti-mouse CD45, APC-Cy7 conjugated, clone: 30-F11(BD PharMingen, 557659). Anti-mouse CD3e, PerCP-Cy5.5 conjugated, clone: 145–2C11 (BD PharMingen, 551163). Anti-mouse CD8a, FITC conjugated, clone: 53-6.7 (BD PharMingen, 553031). Anti-mouse CD4, FITC conjugated, clone: RM4-5 (BD PharMingen, 553047). Anti-mouse CD11c, PE conjugated, clone: HL3 (BD PharMingen, 553802). Anti-mouse CD103, BV421 conjugated, clone: M290 (BD PharMingen, 562771). Anti-mouse F4/80, FITC conjugated, clone: BM8 (Biolegend, 123108). Anti-mouse B220, FITC conjugated, clone: RA3–6B2 (Biolegend, 103206). Anti-mouse I-A/I-E (MHCII) Antibody, PE-Cy7 conjugated, clone: M5/114.15.2 (Biolegend, 107628). Anti-mouse CD8a, APC conjugated, clone: 53-6.7 (BD PharMingen, 553035). Non-viable cells were excluded from further flow analysis using a Live/Dead Fixable Violet Dead Cell Stain Kit (ThermoFisher, L34955) or Aqua Dead Cell Stain Kit (ThermoFisher, L34966). FoxP3 staining was conducted per the manufacturers protocol using the mouse FoxP3 Buffer Set (BD Biosciences, 560409). Data were analyzed using FlowJo version 10. All gating strategies are described in Figure S6D.

Protoporphyrin IX flow cytometry—DC2.4 or $Braf^{V600E}Pten^{-/-}$melanoma cells were cultured for 48 hours with OMP-18R5 and/or recombinant Wnt5a (R&D systems, 645-WN-010), terminally incubated for 4 hours with aminolevulenic acid (Sigma-Aldrich, A3785) followed by flow cytometry (BD For-tessa II) as previously described (Zhao et al., 2018b).

Immunohistochemistry—Tissues were paraffin embedded and processed following standard protocols and imaged with a Zeiss CLSM 700 confocal micro-scope. For Lung and Tumor H&E, hematoxylin (VWR, 95057–844) was stained followed by Eosin (VWR, 95057–848). The following antibodies were used for Immunohistochemistry: Rabbit anti-mouse CD8α (D4W2Z) 1:400 (Cell Signaling, 98941), anti-mouse CXCL5 1:200 (LsBio, LS-C104413), rat anti-mouse Ly6g 1:100 (Abcam, ab25377), rabbit anti-mouse β-catenin 1:100 (Cell signaling, 8480). Antigen retrieval was performed by incubation in BioCare's Nexgen Decloaker chamber for 20 minutes at 90°C. Anti-rabbit polymers were used as secondary antibodies and Vina Green Chromogen Kit (Biocare Medical, BRR 807 AH) was used as substrate for CD8. For CXCL5, LY6G, and β-catenin, anti-rat or rodent polymers were used as secondary antibodies, and Warp Red Chromagen Kit (Biocare Medical, 901-WR806–081017) was used as substrate. ImageJ software was used for quantification.

Western blot—Tumor tissue or cells were homogenized in 1% NP40 lysis buffer (Sigma-Aldrich, 492016) or RIPA Lysis and Extraction Buffer (ThermoFisher, 89901) supplemented with complete protease inhibitor and phosphatase inhibitor (Roche, 4693159001 and 4906845001). Protein samples were separated by SDS-PAGE and transferred onto PVDF/Nitrocellulose membranes (Bio-Rad). Mono/polyclonal primary antibodies and appropriate HRP-conjugated secondary antibodies were used for blotting. The proteins were visualized by ECL-Plus (GE Healthcare) using the Syngene G Box system (Syngene) or ImageQuant

LAS 500 (GE HealthcareLife Sciences). The following antibodies were used: IDO1 (mIDO-48, Santa Cruz Biotechnology, sc-53978) 1:500 overnight at 4°C, TDO2 (Proteintech, 15880–1-AP) 1:500 for 1.5 hours at room temperature), β-Catenin (Cell Signaling, 8480S) 1:1000 overnight at 4°C.

ELISA—Tumors, TDLNs, and non-TDLNs were harvested, flash frozen in liquid nitrogen for −80°C storage and later processed via homogenization by mechanical dissociation with gentleMACS Tissue Dissociator (Miltenyi Biotec, 130-093-235) in M tubes (Miltenyi, 130-093-236). ELISA was performed using (MyBioSource, MBS043489) per the manufacturer's instructions.

ELISPOT assays—Mouse IFNγ ELISPOTPLUS (MABTECH) was performed according to the manufacturer's guidelines. In brief, single-cell suspensions of splenocytes, generated by mechanical dissociation followed by RBC lysis using ammonium chloride, were plated at 2.5×10^5-1×10^6 cells/well on an ELISPOT plate (MABTECH, 3321–4APT-2) and incubated for 24 hours at 37°C with the following peptides: TRP2180–188 peptide (1 mg/mL, SVYDFFVWL; ANASPEC, AS-61058) for melanoma experiments, MUT151–58 peptide (1 mg/mL, FEQNTAQP; BACHEM, 4026648) for Lewis Lung Carcinoma experiments, ConA-positive control, or the irrelevant negative control OVA257–264 peptide (1 mg/mL, SIINFEKL, InvivoGen). To perform the tumor cell lysate ELISPOT assay for the KP autochthonous lung cancer experiment, we modified a previously described method. Briefly, 10^7 monolayer cultures were trypsinized, washed with cold PBS thrice, and resuspended in 1 mL of PBS. The cells were frozen and thawed four times, and the lysate was centrifuged at 300 g for 10 min. The supernatant concentration was determined using a Pierce BCA Protein Assay Kit (Thermo Fisher, 23227). Tumor lysate was added to splenocytes at a final concentration of 120 μg/mL and incubated for 24 hours. Imaging was conducted using a CTL ImmunoSpot S5 core (ImmunoSpot) and quantified using ImmunoCapture and ImmunoSpot software (ImmunoSpot).

Treg assay—BMDCs from BALB/c mice were treated with either OMP-18R5 or OMP-54F28 for 2 hours followed by treatment with Wnt5a (200 ng/mL) (R&D systems) for 48 hours. For $Braf^{V600E}Pten^{-/-}$melanoma cell line derived conditioned-media, melanoma cells were treated with C59 at 100 nmol/L (Selleckchem, S7037) or DMSO control for 48 hours, followed by stimulation of BMDCs as previously described (Holtzhausen et al., 2015) for 48 hours. BMDCs were washed and CD11c selection was performed using the Miltenyi CD11c magnetic selection columns (Miltenyi, 130-108-338) then co-cultured at a ratio of 1:5 with naive $CD4^+$ T cells selected from the spleens of FoxP3-GFP reporter mice processed per the manufacturer protocol (StemCell Technologies, Inc., 19765). After 5–6 days of co-culture, flow cytometry was performed to quantify $FoxP3^+CD4^+$ T cells as previously described (Zhao et al., 2018b).

$CD11c^+$ DC purification and qRT-PCR analysis—TDLNs were taken at the time of experiment termination and digested in RPMI with collagenase (1 g/100mL HBSS, 10x stock, Sigma-Aldrich, C-5138) and DNase (20,000 U/100mL HBSS, 10x stock solution, Sigma-Aldrich, D-5025) at 37°C at 250 rpm in 15 mL conical tubes for 15 minutes. Lymph

nodes were processed through a 40 μM cell strainer (Corning, 431750) and CD11c selection was performed using the Miltenyi CD11c magnetic selection columns (Miltenyi, 130-108-338), per the manufacturer's instructions ($CD11c^+$ DC purity was verified to be > 95% by flow cytometry). Selected cells were washed with PBS and lysed with RLT PLUS (QIAGEN, 1053393) with β-mercaptoethanol (VWR, VWRV0482–250ML). RNA was isolated using the RNAeasy Plus Micro kit (QIAGEN, 74034) per the manufacturer's instructions. cDNA was generated using the SuperScript IV FirstStrand Synthesis System (Invitrogen, 11756050) and qRT-PCR was performed on an AB 7500 Real-Time PCR Instrument (Life Technologies) using the PowerUp Master Mix (Applied Biosciences, A25742). Ct values were normalized to GAPDH using the $^{\Delta\Delta}$Ct method.

Tumor RNA isolation and qRT-PCR—Flash frozen tumors were processed with M-tubes (Miltenyi, 130-093-236) in RLT PLUS (QIAGEN, 1053393) with β-mercaptoethanol (VWR, VWRV0482–250ML). Tumor biopsies taken prior to anti-PD-1 escape were taken and directly lysed in RLT PLUS. RNA was isolated and cDNA generated as above. Ct values were normalized to β-actin using the $^{\Delta\Delta}$Ct method.

Lung imaging and analysis—KP mice were imaged for tumor development by serial micro-CT at 2-week intervals beginning 10 weeks post infection as previously described (Perez et al., 2013; Torok et al., 2019). Briefly, the XRAD225 Cx (Precision X-Ray, Inc.) small-animal image-guided irradiator was used for serial micro-CT. Mice were placed in a prone position and anesthetized with isoflurane via nose cone delivery system. Mice were breathing freely during image acquisition, thus tumor volumes represented an internal target volume that integrated changes over the respiratory cycle. For CT acquisition to image the lungs 40 kVP, 2.5 mA X-rays were used with a 2-mm Al filter, and images were analyzed using the Amira 3D Visualization and Analysis Software Suite (FEI, ThermoFisher Scientific) to calculate tumor volumes as further described elsewhere (Torok et al., 2019). Each individual lesion was contoured to calculate the tumor volume. In most mice, multiple target lesions were identified. Target lesion volume was subsequently measured every 2 weeks and normalized to the volume at baseline to calculate fold changes in tumor volume. Target lesions obscured by other anatomic changes were excluded.

Kynurenine LC-MS/MS—LC-MS/MS was performed by the Duke Pharmacokinetics/Pharmacodynamics core facility. Kyn-KynA-Trp working solutions were as followed: Kyn stock solution (SS1): 5 μg/mL, Trp stock solution (SS2): 1 mg/mL, KynA stock solution (SSA): 20 μg/mL. The following calibration curves were: Kyn: 2.6 – 100 ng/mL, KynA: 0.5–20 ng/mL, Trp: 0.5–20 μg/mL. Drug extraction was performed on tumor homogenate consisting of 1x tissue and 2x H_2O. 60 μL IS (100 ng/mL Kyn-d4+ 1 ug/mL Trp-d5+20 ng/mL KynA-d5) in mphA was added to 20 μl of homogenate. 200 μl of CH_3Cl was then added to mixture. Samples were homogenized/extracted on "Fast Prep" at Speed 4.0 for 20 s and centrifuged for 5 minutes at 16,000 g. For Trp, 2 μL of supernatant was transferred into an injection vial, 40 μL of mphA was added, and the sample was vortexed, centrifuged, and 5μl was injected. For Kyn/KynA: the leftover supernatant was transferred into another injection vial. Samples were then run on 4000Q LC/MS/MS system at 4°C. Example chromatographs are demonstrated in Figure S5F.

RNaseq dataset re-analysis—RNA-seq data from Hugo et al. (GEO: GSE78220) (Hugo et al., 2016) was processed using the TrimGalore toolkit which employs Cutadapt to trim low-quality bases and Illumina sequencing adapters from the 3′ end of the reads. Only reads that were 20nt or longer after trimming were kept for further analysis. Reads were mapped to the GRCh37v73 version of the human genome and transcriptome using the STAR RNA-seq alignment tool. Reads were kept for subsequent analysis if they mapped to a single genomic location. Gene counts were compiled using the HTSeq tool. Only genes that had at least 10 reads in any given library were used in subsequent analysis. Normalization and differential expression were carried out using the DESeq26 Bioconductor package with the R statistical programming environment. We included batch and sex as cofactors in the differential expression model. The false discovery rate was calculated to control for multiple hypothesis testing. Gene set enrichment analysis was performed to identify differentially regulated pathways and gene ontology terms for each of the comparisons performed. Wnt pathway focused re-analysis was performed on RNaseq from autochthonous mouse melanomas treated with IgG or anti-PD-1 as previously described (50-bp single-read sequencing; Anti–PD-1 resistance Study RNA-seq, accession number: SAMN09878780) (Zhao et al., 2018a). Heatmaps were generated using the heatmap.2 function in *R*.

NanoString—Archival melanoma specimens of patients treated with anti-PD-1 (either pembrolizumab or nivolumab) monotherapy were obtained via an ongoing clinical trial (ClinicalTrials.gov: NCT02694965). After verification by a board-certified pathologist, microdissection was performed if deemed necessary. Two-to-three 10 μM FFPE scrolls were collected from FFPE sectioning of biopsies taken prior to treatment, and RNA extraction was performed using RSC FFPE RNA extraction kit (Promega) according to manufacturer's instruction. Agilent 2100 Bioanalyzer (Agilent) and NanoDrop (ThermoFisher) were used to determine the purity and concentration of the RNA. A DV300 Agilent Bioanalyzer smear analysis was used to determine the percentage of fragments greater than 300 nucleotides to determine the starting amount of RNA. Samples were analyzed on a NanoString nCounter Max system using the nCounter Vantage 3D Human Wnt Pathways Panel (N2_WNT_Pth_v1.0), which is comprised of Wnt ligands, receptors, regulators, gene targets, and other pathway components with the addition of a custom gene panel composed of cytolytic T cell markers and *IDO1*. Gene expression codesets (designed and produced by NanoString Technologies, Seattle, WA), hybridization buffer and total RNA were hybridized in a thermocycler for 16 hours at 67°C prior to being processed in the nCounter Max Prep Station following the NanoString manual, MAN-10056–02 for gene expression assays. Data collection using the nCounter Digital Analyzer was performed by following the NanoString manual, MAN-C0035–07 using the maximum field of view setting. Analysis was performed using the nSolver software (NanoString). Tumor specimen samples from the multi-site, international, phase I advanced solid tumor ETC-159 clinical trial (ClinicalTrials.gov: NCT02521844, A*STAR Research Entities, Singapore), were analyzed using the PanCancer IO panel (NS_CANCERIMMUNE_) which contains immune genes including cytokines, chemokines, myeloid cells, T-, B-, and NK-cells, and genes associated with antigen processing.

QUANTIFICATION AND STATISTICAL ANALYSIS

GraphPad Prism 7 Windows version was used for all statistical analyses. Unpaired two-sided Student's t tests were used to compare mean differences between control and treatment groups. Univariate ANOVA followed by Tukey post hoc test was performed to analyze data containing three or more groups. Kaplan-Meier estimates were utilized for survival analyses. The Benjamini-Yekutieli method of correction was utilized to control the false-discovery rate (FDR) associated with the Nanostring transcriptional data analysis. The significance threshold for all statistical calculations was based on a *P value* of 0.05, and all tests were two-sided. All quantitative data is presented as a mean and associated SEM. Number of replicates and individual tests used can be found in the figure legends. Mice were allocated to treatment groups to maintain similar average initial tumor sizes in each group. No data was excluded in described studies.

ADDITIONAL RESOURCES

Archival melanoma specimens of patients treated with anti-PD-1 (either pembrolizumab or nivolumab) monotherapy were obtained via an ongoing clinical trial (ClinicalTrials.gov: NCT02694965). Patient samples were also obtained from the completed multi-site, international, phase I advanced solid tumor ETC-159 clinical trial (ClinicalTrials.gov: NCT02521844, A*STAR Research Entities, Singapore).

Supplementary Material

Refer to Web version on PubMed Central for supplementary material.

ACKNOWLEDGMENTS

The authors would like to thank John Lewicki, PhD (Mereo BioPharma), Tim Hoey, PhD (Tenaya Therapeutics), and Jakob Dupont, MD, MA (Atara Bio-therapeutics) for guidance and support in executing the described studies utilizing the OMP-18R5 and OMP-54F28 Wnt ligand inhibitors. We would also like to recognize Mike Cook, PhD of the Duke Cancer Institute Flow Cytometry Shared Resource, Ivan Spasojevic, PhD of the Duke Cancer Institute Pharmacokinetics and Pharmacodynamics Core Laboratory, and David Kirsch, MD, PhD and his laboratory in the Duke Department of Radiation Oncology for assistance with the KP mouse model; Holly Dressman, PhD of the Duke Center for Genomic and Computational Biology and Andrea Roche, MA, Software Developer of SAS Institute, for assistance with heatmap design and R code; Mark Berrong of the Innate and Adaptive Cellular Cytotoxicity Laboratory for assistance with ELISpot quantification; and members of the Duke Clinical Melanoma Research Team for assistance with the melanoma tissue acquisition protocol. This work was supported in part by a Damon Runyon Physician Scientist Award (to N.C.D.); NIH F32 1F32CA247067-01A1 (to M.P.P.), K08 CA191063 (to B.A.H.), R37 CA249085 (to B.A.H.); a Duke University Health Scholar Award (to B.A.H.); a Duke Strong Start Award (to B.A.H.); the Ross Bierkan Melanoma Fund (to B.A.H. and A.K.S.S.); a pre-clinical research grant from OncoMed Pharmaceuticals, Inc. (to B.A.H.); a pre-clinical research grant from the Agency for Science, Technology, and Research, Singapore (A*STAR) (to B.A.H.); and by a pre-clinical research grant from Merck (to B.A.H). Parts of this study were funded by the National Medical Research Council, Singapore (NMRC), the National Research Foundation of Singapore (NRF), and by the Biomedical Research Council of Singapore (BMRC).

DECLARATION OF INTERESTS

A.K.S. received research funding from Bristol Myers Squibb, Immunocore, and Merck. J.H.S. received research funding from A*STAR Singapore, Curegenix, and Leap. J.H.S. has also received research funding and served on the scientific advisory board for OncoMed. B.A.H. received research funding from OncoMed, Merck, and Leap. B.A.H., N.C.D., and B.T. are authors on a patent describing paracrine Wnt ligand signaling as a predictive marker for cancer immunotherapy. V.N.D. is an employee of EDDC/A*STAR and is an author on a patent on combining ETC-159 with pembrolizumab. The remaining authors declare no competing interests.

REFERENCES

Bagby SM, Hartman SJ, Navarro NM, Yacob BW, Shulman J, Barkow J, Lieu CH, Davis SL, Leal AD, Messersmith WA, et al. (2020). Sensitizing microsatellite stable colorectal cancer to immune checkpoint therapy utilizing Wnt pathway inhibition. Cancer Res. 80 (16, Suppl), 6647. https://cancerres.aacrjournals.org/content/80/16_Supplement/6647.

Brinkmann EM, Mattes B, Kumar R, Hagemann AI, Gradl D, Scholpp S, Steinbeisser H, Kaufmann LT, and Özbek S (2016). Secreted frizzled-related protein 2 (sFRP2) redirects non-canonical wnt signaling from Fz7 to Ror2 during vertebrate gastrulation. J. Biol. Chem 291, 13730–13742. [PubMed: 27129770]

Chaudhary B, and Elkord E (2016). Regulatory T cells in the tumor microenvironment and cancer progression: Role and therapeutic targeting. Vaccines (Basel) 4, 28.

Clevers H, and Nusse R (2012). Wnt/β-catenin signaling and disease. Cell 149, 1192–1205. [PubMed: 22682243]

Damsky WE, Curley DP, Santhanakrishnan M, Rosenbaum LE, Platt JT, Gould Rothberg BE, Taketo MM, Dankort D, Rimm DL, McMahon M, and Bosenberg M (2011). β-Catenin signaling controls metastasis in Braf-activated Pten-deficient melanomas. Cancer Cell 20, 741–754. [PubMed: 22172720]

Davis SL, Cardin DB, Shahda S, Lenz HJ, Dotan E, O'Neil BH, Kapoun AM, Stagg RJ, Berlin J, Messersmith WA, and Cohen SJ (2020). A phase 1b dose escalation study of Wnt pathway inhibitor vantictumab in combination with nab-paclitaxel and gemcitabine in patients with previously untreated metastatic pancreatic cancer. Invest. New Drugs 38, 821–830. [PubMed: 31338636]

DuPage M, Dooley AL, and Jacks T (2009). Conditional mouse lung cancer models using adenoviral or lentiviral delivery of Cre recombinase. Nat. Protoc 4, 1064–1072. [PubMed: 19561589]

Fischer MM, Cancilla B, Yeung VP, Cattaruzza F, Chartier C, Murriel CL, Cain J, Tam R, Cheng CY, Evans JW, et al. (2017). WNT antagonists exhibit unique combinatorial antitumor activity with taxanes by potentiating mitotic cell death. Sci. Adv 3, e1700090. [PubMed: 28691093]

Forsthuber A, Lipp K, Andersen L, Ebersberger S, Graña-Castro, Ellmeier W, Petzelbauer P, Lichtenberger BM, and Loewe R (2019). CXCL5 as regulator of neutrophil function in cutaneous melanoma. J. Invest. Dermatol 139, 186–194. [PubMed: 30009831]

Garon EB, Rizvi NA, Hui R, Leighl N, Balmanoukian AS, Eder JP, Patnaik A, Aggarwal C, Gubens M, Horn L, et al.; KEYNOTE-001 Investigators (2015). Pembrolizumab for the treatment of non-small-cell lung cancer. N. Engl. J. Med 372, 2018–2028. [PubMed: 25891174]

Garris CS, Arlauckas SP, Kohler RH, Trefny MP, Garren S, Piot C, Engblom C, Pfirschke C, Siwicki M, Gungabeesoon J, et al. (2018). Successful anti-PD-1 cancer immunotherapy requires T cell-dendritic cell cross-talk involving the cytokines IFN-γ and IL-12. Immunity 49, 1148–1161.e7. [PubMed: 30552023]

Gide TN, Wilmott JS, Scolyer RA, and Long GV (2018). Primary and acquired resistance to immune checkpoint inhibitors in metastatic melanoma. Clin. Cancer Res 24, 1260–1270. [PubMed: 29127120]

Gurney A, Axelrod F, Bond CJ, Cain J, Chartier C, Donigan L, Fischer M, Chaudhari A, Ji M, Kapoun AM, et al. (2012). Wnt pathway inhibition via the targeting of Frizzled receptors results in decreased growth and tumorigenicity of human tumors. Proc. Natl. Acad. Sci. USA 109, 11717–11722. [PubMed: 22753465]

Hamid O, Schmidt H, Nissan A, Ridolfi L, Aamdal S, Hansson J, Guida M, Hyams DM, Gómez H, Bastholt L, et al. (2011). A prospective phase II trial exploring the association between tumor microenvironment biomarkers and clinical activity of ipilimumab in advanced melanoma. J. Transl. Med 9, 204. [PubMed: 22123319]

Highfill SL, Cui Y, Giles AJ, Smith JP, Zhang H, Morse E, Kaplan RN, and Mackall CL (2014). Disruption of CXCR2-mediated MDSC tumor trafficking enhances anti-PD1 efficacy. Sci. Transl. Med 6, 237ra67.

Holmgaard RB, Zamarin D, Li Y, Gasmi B, Munn DH, Allison JP, Merghoub T, and Wolchok JD (2015). Tumor-expressed IDO recruits and activates MDSCs in a Treg-dependent manner. Cell Rep. 13, 412–424. [PubMed: 26411680]

Holtzhausen A, Zhao F, Evans KS, Tsutsui M, Orabona C, Tyler DS, and Hanks BA (2015). Melanoma-derived Wnt5a promotes local dendritic-cell expression of IDO and immunotolerance: opportunities for pharmacologic enhancement of immunotherapy. Cancer Immunol. Res 3, 1082–1095. [PubMed: 26041736]

Hong Y, Manoharan I, Suryawanshi A, Majumdar T, Angus-Hill ML, Koni PA, Manicassamy B, Mellor AL, Munn DH, and Manicassamy S (2015a). β-Catenin promotes regulatory T-cell responses in tumors by inducing vitamin A metabolism in dendritic cells. Cancer Res. 75, 656–665. [PubMed: 25568183]

Hong Y, Manoharan I, Suryawanshi A, Shanmugam A, Swafford D, Ahmad S, Chinnadurai R, Manicassamy B, He Y, Mellor AL, et al. (2015b). Deletion of LRP5 and LRP6 in dendritic cells enhances antitumor immunity. OncoImmunology 5, e1115941. [PubMed: 27141399]

Hou DY, Muller AJ, Sharma MD, DuHadaway J, Banerjee T, Johnson M, Mellor AL, Prendergast GC, and Munn DH (2007). Inhibition of indoleamine 2,3-dioxygenase in dendritic cells by stereoisomers of 1-methyl-tryptophan correlates with antitumor responses. Cancer Res. 67, 792–801. [PubMed: 17234791]

Hugo W, Zaretsky JM, Sun L, Song C, Moreno BH, Hu-Lieskovan S, Berent-Maoz B, Pang J, Chmielowski B, Cherry G, et al. (2016). Genomic and transcriptomic features of response to anti-PD-1 therapy in metastatic melanoma. Cell 165, 35–44. [PubMed: 26997480]

Inaba K, Inaba M, Romani N, Aya H, Deguchi M, Ikehara S, Muramatsu S, and Steinman RM (1992). Generation of large numbers of dendritic cells from mouse bone marrow cultures supplemented with granulocyte/macro-phage colony-stimulating factor. J. Exp. Med 176, 1693–1702. [PubMed: 1460426]

Janku F, Connolly R, LoRusso P, de Jonge M, Vaishampayan U, Rodon J, Argilés G, Myers A, Schmitz SFH, Ji Y, et al. (2015). Phase I study of WNT974, a first-in-class porcupine inhibitor, in advanced solid tumors. Mol. Cancer Ther 14 (12, Suppl 2), C45. https://mct.aacrjournals.org/content/14/12_Supplement_2/C45.

Janku F, de Vos F, de Miguel M, Forde P, Ribas A, Nagasaka M, Argiles G, Arance AM, Calvo A, Giannakis M, et al. (2020). Phase I study of WNT974 + spartalizumab in patients (pts) with advanced solid tumors. Cancer Res. 80 (16, Suppl), CT034. https://cancerres.aacrjournals.org/content/80/16_Supplement/CT034.

Jimeno A, Gordon M, Chugh R, Messersmith W, Mendelson D, Dupont J, Stagg R, Kapoun AM, Xu L, Uttamsingh S, et al. (2017). A first-in-human phase I study of the anticancer stem cell agent ipafricept (OMP-54F28), a decoy receptor for Wnt ligands, in patients with advanced solid tumors. Clin. Cancer Res 23, 7490–7497. [PubMed: 28954784]

Jung YS, and Park JI (2020). Wnt signaling in cancer: Therapeutic targeting of Wnt signaling beyond β-catenin and the destruction complex. Exp. Mol. Med 52, 183–191. [PubMed: 32037398]

Katoh M, and Katoh M (2007). WNT signaling pathway and stem cell signaling network. Clin. Cancer Res 13, 4042–4045. [PubMed: 17634527]

Krishnamurthy N, and Kurzrock R (2018). Targeting the Wnt/beta-catenin pathway in cancer: Update on effectors and inhibitors. Cancer Treat. Rev 62, 50–60. [PubMed: 29169144]

Lescher B, Haenig B, and Kispert A (1998). *sFRP-2* is a target of the Wnt-4 signaling pathway in the developing metanephric kidney. Dev. Dyn 213, 440–451. [PubMed: 9853965]

Lewis-Ballester A, Forouhar F, Kim SM, Lew S, Wang Y, Karkashon S, Seetharaman J, Batabyal D, Chiang BY, Hussain M, et al. (2016). Molecular basis for catalysis and substrate-mediated cellular stabilization of human tryptophan 2,3-dioxygenase. Sci. Rep 6, 35169. [PubMed: 27762317]

Li X, Liu P, Liu W, Maye P, Zhang J, Zhang Y, Hurley M, Guo C, Boskey A, Sun L, et al. (2005). Dkk2 has a role in terminal osteoblast differentiation and mineralized matrix formation. Nat. Genet 37, 945–952. [PubMed: 16056226]

Long GV, Dummer R, Hamid O, Gajewski TF, Caglevic C, Dalle S, Arance A, Carlino MS, Grob JJ, Kim TM, et al. (2019). Epacadostat plus pembrolizumab versus placebo plus pembrolizumab in patients with unresectable or metastatic melanoma (ECHO-301/KEYNOTE-252): A phase 3, randomised, double-blind study. Lancet Oncol. 20, 1083–1097. [PubMed: 31221619]

Luke JJ, Bao R, Sweis RF, Spranger S, and Gajewski TF (2019). WNT/β-catenin pathway activation correlates with immune exclusion across human cancers. Clin. Cancer Res 25, 3074–3083. [PubMed: 30635339]

Mandelboim O, Berke G, Fridkin M, Feldman M, Eisenstein M, and Eisenbach L (1994). CTL induction by a tumour-associated antigen octapeptide derived from a murine lung carcinoma. Nature 369, 67–71. [PubMed: 8164742]

Manicassamy S, Reizis B, Ravindran R, Nakaya H, Salazar-Gonzalez RM, Wang YC, and Pulendran B (2010). Activation of β-catenin in dendritic cells regulates immunity versus tolerance in the intestine. Science 329, 849–853. [PubMed: 20705860]

Marvel D, and Gabrilovich DI (2015). Myeloid-derived suppressor cells in the tumor microenvironment: Expect the unexpected. J. Clin. Invest 125, 3356–3364. [PubMed: 26168215]

Metz R, Duhadaway JB, Rust S, Munn DH, Muller AJ, Mautino M, and Prendergast GC (2010). Zinc protoporphyrin IX stimulates tumor immunity by disrupting the immunosuppressive enzyme indoleamine 2,3-dioxygenase. Mol. Cancer Ther 9, 1864–1871. [PubMed: 20530717]

Meyer C, Cagnon L, Costa-Nunes CM, Baumgaertner P, Montandon N, Leyvraz L, Michielin O, Romano E, and Speiser DE (2014). Frequencies of circulating MDSC correlate with clinical outcome of melanoma patients treated with ipilimumab. Cancer Immunol. Immunother 63, 247–257. [PubMed: 24357148]

Mieszczanek J, de la Roche M, and Bienz M (2008). A role of Pygopus as an anti-repressor in facilitating Wnt-dependent transcription. Proc. Natl. Acad. Sci. USA 105, 19324–19329. [PubMed: 19036929]

Mlecnik B, Bindea G, Angell HK, Maby P, Angelova M, Tougeron D, Church SE, Lafontaine L, Fischer M, Fredriksen T, et al. (2016). Integrative analyses of colorectal cancer show immunoscore is a stronger predictor of patient survival than microsatellite instability. Immunity 44, 698–711. [PubMed: 26982367]

Moore KN, Gunderson CC, Sabbatini P, McMeekin DS, Mantia-Smaldone G, Burger RA, Morgan MA, Kapoun AM, Brachmann RK, Stagg R, et al. (2019). A phase 1b dose escalation study of ipafricept (OMP54F28) in combination with paclitaxel and carboplatin in patients with recurrent platinum-sensitive ovarian cancer. Gynecol. Oncol 154, 294–301. [PubMed: 31174889]

Muller AJ, DuHadaway JB, Donover PS, Sutanto-Ward E, and Prendergast GC (2005). Inhibition of indoleamine 2,3-dioxygenase, an immunoregulatory target of the cancer suppression gene *Bin1*, potentiates cancer chemotherapy. Nat. Med 11, 312–319. [PubMed: 15711557]

Muller AJ, Manfredi MG, Zakharia Y, and Prendergast GC (2019). Inhibiting IDO pathways to treat cancer: lessons from the ECHO-301 trial and beyond. Semin. Immunopathol 41, 41–48. [PubMed: 30203227]

Munn DH (2012). Blocking IDO activity to enhance anti-tumor immunity. Front. Biosci. (Elite Ed.) 4, 734–745. [PubMed: 22201909]

Munn DH, and Mellor AL (2007). Indoleamine 2,3-dioxygenase and tumor-induced tolerance. J. Clin. Invest 117, 1147–1154. [PubMed: 17476344]

Munn DH, and Mellor AL (2016). IDO in the tumor microenvironment: Inflammation, counter-regulation, and tolerance. Trends Immunol. 37, 193–207. [PubMed: 26839260]

Patel SA, and Minn AJ (2018). Combination cancer therapy with immune checkpoint blockade: Mechanisms and strategies. Immunity 48, 417–433. [PubMed: 29562193]

Perez BA, Ghafoori AP, Lee CL, Johnston SM, Li Y, Moroshek JG, Ma Y, Mukherjee S, Kim Y, Badea CT, and Kirsch DG (2013). Assessing the radiation response of lung cancer with different gene mutations using genetically engineered mice. Front. Oncol 3, 72. [PubMed: 23565506]

Pfirschke C, Engblom C, Rickelt S, Cortez-Retamozo V, Garris C, Pucci F, Yamazaki T, Poirier-Colame V, Newton A, Redouane Y, et al. (2016). Immunogenic chemotherapy sensitizes tumors to checkpoint blockade therapy. Immunity 44, 343–354. [PubMed: 26872698]

Prendergast GC, Malachowski WP, DuHadaway JB, and Muller AJ (2017). Discovery of IDO1 inhibitors: From bench to bedside. Cancer Res. 77, 6795–6811. [PubMed: 29247038]

Reck M, Rodríguez-Abreu D, Robinson AG, Hui R, Csőszi T, Fülö p A, Gottfried M, Peled N, Tafreshi A, Cuffe S, et al.; KEYNOTE-024 Investigators (2016). Pembrolizumab versus chemotherapy for

PD-L1-positive non-small-cell lung cancer. N. Engl. J. Med 375, 1823–1833. [PubMed: 27718847]

Ring L, Peröbner I, Karow M, Jochum M, Neth P, and Faussner A (2011). Reporter gene HEK 293 cells and WNT/Frizzled fusion proteins as tools to study WNT signaling pathways. Biol. Chem 392, 1011–1020. [PubMed: 21864196]

Robert C, Schachter J, Long GV, Arance A, Grob JJ, Mortier L, Daud A, Carlino MS, McNeil C, Lotem M, et al.; KEYNOTE-006 investigators (2015). Pembrolizumab versus ipilimumab in advanced melanoma. N. Engl. J. Med 372, 2521–2532. [PubMed: 25891173]

Sade-Feldman M, Kanterman J, Klieger Y, Ish-Shalom E, Olga M, Saragovi A, Shtainberg H, Lotem M, and Baniyash M (2016). Clinical significance of circulating $CD33^{+}CD11b^{+}$HLA-DR myeloid cells in patients with stage IV melanoma treated with ipilimumab. Clin. Cancer Res 22, 5661–5672. [PubMed: 27178742]

Salmon H, Idoyaga J, Rahman A, Leboeuf M, Remark R, Jordan S, Casanova-Acebes M, Khudoynazarova M, Agudo J, Tung N, et al. (2016). Expansion and activation of $CD103^{+}$ dendritic cell progenitors at the tumor site enhances tumor responses to therapeutic PD-L1 and BRAF inhibition. Immunity 44, 924–938. [PubMed: 27096321]

Sánchez-Paulete AR, Cueto FJ, Martínez-López M, Labiano S, Morales-Kastresana A, Rodríguez-Ruiz ME, Jure-Kunkel M, Azpilikueta A, Aznar MA, Quetglas JI, et al. (2016). Cancer immunotherapy with immunomodulatory anti-CD137 and anti-PD-1 monoclonal antibodies requires BATF3-dependent dendritic cells. Cancer Discov. 6, 71–79. [PubMed: 26493961]

Schoenfeld AJ, and Hellmann MD (2020). Acquired resistance to immune checkpoint inhibitors. Cancer Cell 37, 443–455. [PubMed: 32289269]

Sharma P, Hu-Lieskovan S, Wargo JA, and Ribas A (2017). Primary, adaptive, and acquired resistance to cancer immunotherapy. Cell 168, 707–723. [PubMed: 28187290]

Shen Z, Reznikoff G, Dranoff G, and Rock KL (1997). Cloned dendritic cells can present exogenous antigens on both MHC class I and class II molecules. J. Immunol 158, 2723–2730. [PubMed: 9058806]

Simpson TR, Li F, Montalvo-Ortiz W, Sepulveda MA, Bergerhoff K, Arce F, Roddie C, Henry JY, Yagita H, Wolchok JD, et al. (2013). Fc-dependent depletion of tumor-infiltrating regulatory T cells co-defines the efficacy of anti-CTLA-4 therapy against melanoma. J. Exp. Med 210, 1695–1710. [PubMed: 23897981]

Spranger S, Bao R, and Gajewski TF (2015). Melanoma-intrinsic β-catenin signalling prevents anti-tumour immunity. Nature 523, 231–235. [PubMed: 25970248]

Spranger S, Dai D, Horton B, and Gajewski TF (2017). Tumor-residing Batf3 dendritic cells are required for effector T cell trafficking and adoptive T cell therapy. Cancer Cell 31, 711–723.e4. [PubMed: 28486109]

Steele CW, Karim SA, Leach JDG, Bailey P, Upstill-Goddard R, Rishi L, Foth M, Bryson S, McDaid K, Wilson Z, et al. (2016). CXCR2 inhibition profoundly suppresses metastases and augments immunotherapy in pancreatic ductal adenocarcinoma. Cancer Cell 29, 832–845. [PubMed: 27265504]

Sun Y, Zhu D, Chen F, Qian M, Wei H, Chen W, and Xu J (2016). SFRP2 augments WNT16B signaling to promote therapeutic resistance in the damaged tumor microenvironment. Oncogene 35, 4321–4334. [PubMed: 26751775]

Suryawanshi A, Hussein MS, Prasad PD, and Manicassamy S (2020). Wnt signaling cascade in dendritic cells and regulation of anti-tumor immunity. Front. Immunol 11, 122. [PubMed: 32132993]

Tammela T, Sanchez-Rivera FJ, Cetinbas NM, Wu K, Joshi NS, Helenius K, Park Y, Azimi R, Kerper NR, Wesselhoeft RA, et al. (2017). A Wnt-producing niche drives proliferative potential and progression in lung adenocarcinoma. Nature 545, 355–359. [PubMed: 28489818]

Theivanthiran B, Evans KS, DeVito NC, Plebanek M, Sturdivant M, Wachsmuth LP, Salama AK, Kang Y, Hsu D, Balko JM, et al. (2020). A tumor-intrinsic PD-L1/NLRP3 inflammasome signaling pathway drives resistance to anti-PD-1 immunotherapy. J. Clin. Invest 130, 2570–2586. [PubMed: 32017708]

Torok JA, Oh P, Castle KD, Reinsvold M, Ma Y, Luo L, Lee CL, and Kirsch DG (2019). Deletion of *Atm* in tumor but not endothelial cells improves radiation response in a primary mouse model of lung adenocarcinoma. Cancer Res. 79, 773–782. [PubMed: 30315114]

Weber J, Gibney G, Kudchadkar R, Yu B, Cheng P, Martinez AJ, Kroeger J, Richards A, McCormick L, Moberg V, et al. (2016). Phase I/II study of metastatic melanoma patients treated with nivolumab who had progressed after ipilimumab. Cancer Immunol. Res 4, 345–353. [PubMed: 26873574]

Weber R, Fleming V, Hu X, Nagibin V, Groth C, Altevogt P, Utikal J, and Umansky V (2018). Myeloid-derived suppressor cells hinder the anti-cancer activity of immune checkpoint inhibitors. Front. Immunol 9, 1310. [PubMed: 29942309]

Xiao Q, Wu J, Wang WJ, Chen S, Zheng Y, Yu X, Meeth K, Sahraei M, Bothwell ALM, Chen L, et al. (2018). DKK2 imparts tumor immunity evasion through β-catenin-independent suppression of cytotoxic immune-cell activation. Nat. Med 24, 262–270. [PubMed: 29431745]

Yoshida R, Imanishi J, Oku T, Kishida T, and Hayaishi O (1981). Induction of pulmonary indoleamine 2,3-dioxygenase by interferon. Proc. Natl. Acad. Sci. USA 78, 129–132. [PubMed: 6165986]

Zhao F, Evans K, Xiao C, DeVito N, Theivanthiran B, Holtzhausen A, Siska PJ, Blobe GC, and Hanks BA (2018a). Stromal fibroblasts mediate Anti-PD-1 resistance via MMP-9 and dictate TGFβ inhibitor sequencing in melanoma. Cancer Immunol. Res 6, 1459–1471. [PubMed: 30209062]

Zhao F, Xiao C, Evans KS, Theivanthiran T, DeVito N, Holtzhausen A, Liu J, Liu X, Boczkowski D, Nair S, et al. (2018b). Paracrine Wnt5a-β-catenin signaling triggers a metabolic program that drives dendritic cell tolerization. Immunity 48, 147–160.e7. [PubMed: 29343435]

Zhong Z, Sepramaniam S, Chew XH, Wood K, Lee MA, Madan B, and Virshup DM (2019). PORCN inhibition synergizes with PI3K/mTOR inhibition in Wnt-addicted cancers. Oncogene 38, 6662–6677. [PubMed: 31391551]

Highlights

- Proximal Wnt ligand signaling activity is associated with anti-PD-1 resistance
- Wnt signaling drives kynurenine production and PMN-MDSC accumulation in tumors
- Wnt ligand inhibition enhances the efficacy of PD-1 blockade in transgenic models
- Wnt inhibition creates a more favorable immune microenvironment in cancer patients

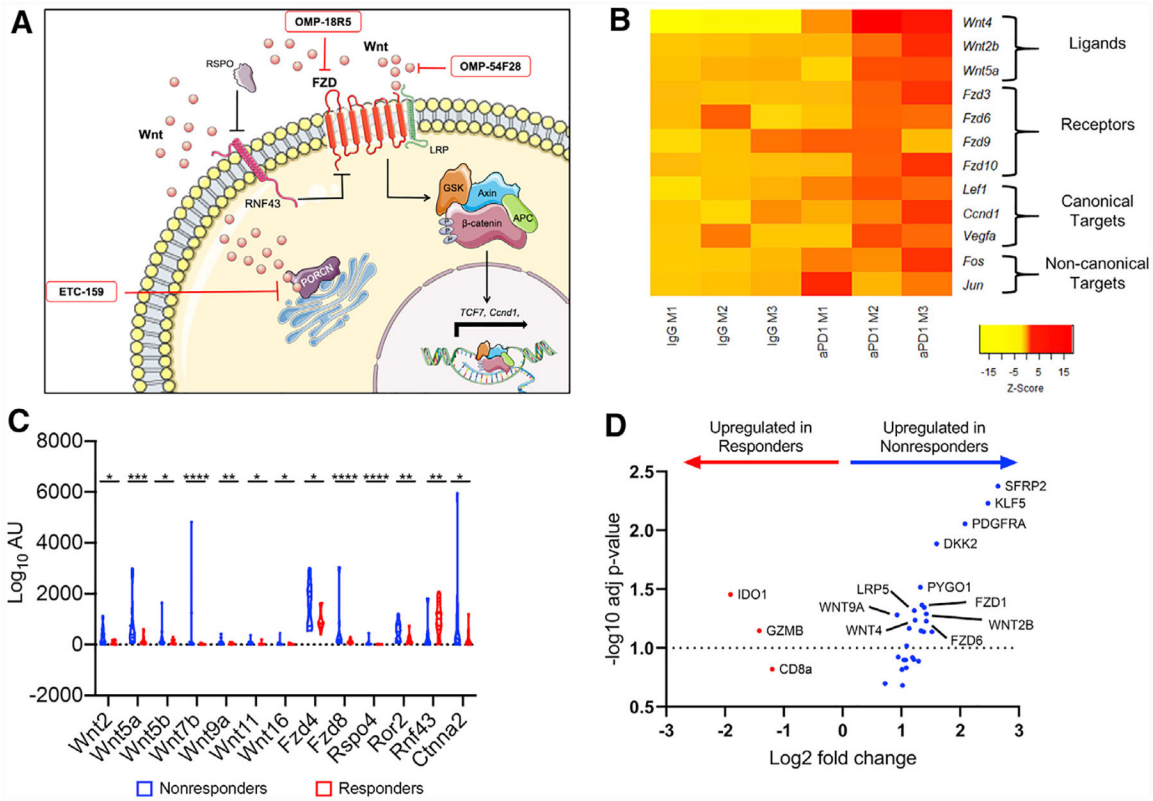

Figure 1. Transcriptomic analysis of Wnt ligands, receptors, and regulators in anti-PD-1 resistance

(A) Schematic of the canonical Wnt signaling pathway and the mechanism of action of OMP-18R5, which blocks Fzd receptors; OMP-54F28 scavenges Wnt ligands; and ETC-159 blocks Wnt ligand secretion by inhibiting PORCN.

(B) Wnt ligand, receptor, and target-focused heatmap generated from RNA-seq analysis of the BP mouse model after aPD1 escape. M, mouse; aPD1, anti-PD-1 antibody.

(C) Reanalysis of RNA-seq data from biopsies of responding (red) and nonresponding (blue) metastatic melanoma patients focused on Wnt ligands, receptors, and regulators (Hugo et al., 2016). AU, arbitrary units. A Student's two-tailed t test was used to compare aPD1 responders versus non-responders. *$p < 0.05$, **$p < 0.01$, ***$p < 0.001$, ****$p < 0.0001$.

(D) Volcano plot of NanoString Wnt pathway analysis of the top 30 differentially expressed genes in metastatic melanoma patients (n = 12 responders, 12 non-responders) prior to receiving aPD1 monotherapy. The Benjamini-Yekutieli method of correction was used for controlling the false discovery rate (FDR), and p values were adjusted based on the total number of comparisons made across the entire gene panel.

See also Tables S1 and S2.

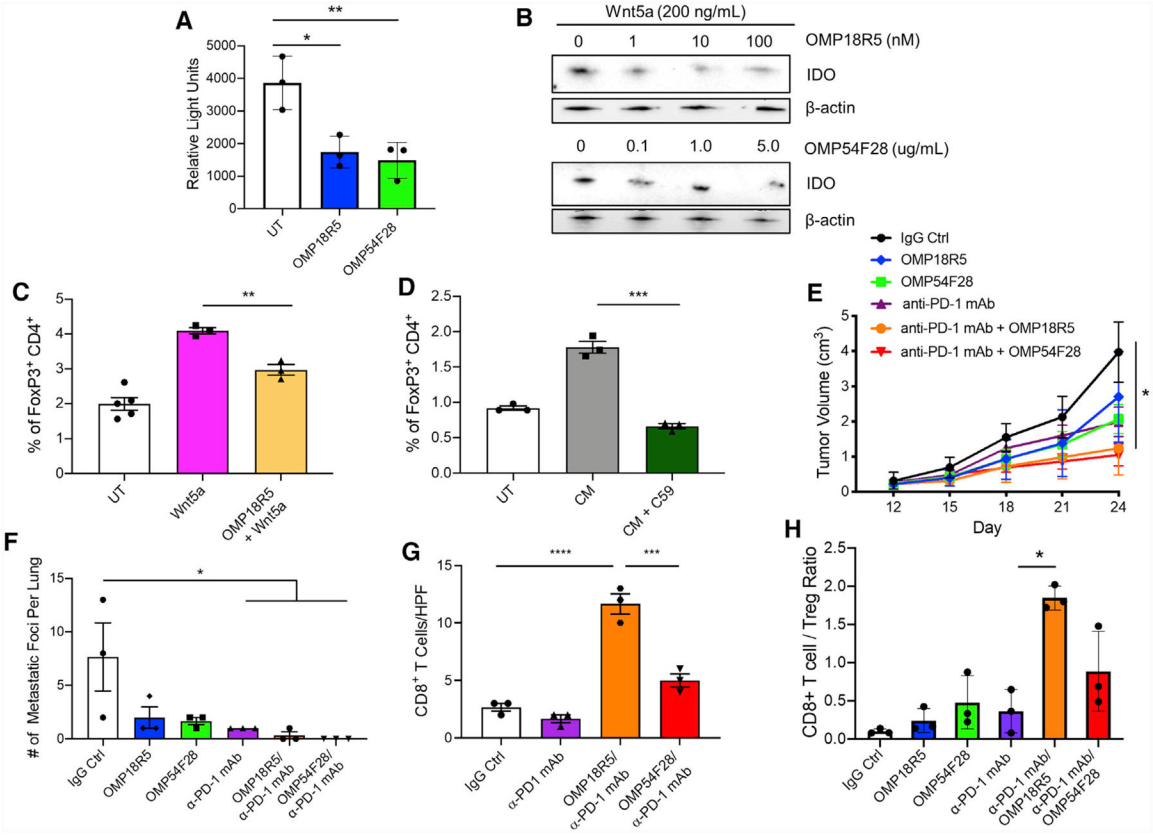

Figure 2. Wnt ligand inhibition reverses Treg generation via IDO1 inhibition and enhances anti-PD-1 therapy in a syngeneic melanoma model

(A) Luciferase assay of the TCF-LEF-luc 293T cell line treated with OMP-18R5 or OMP-54F28. Each condition was performed in triplicate. Data are representative of two independent experiments.

(B) IDO1 western blot analysis of DCs treated with Wnt5a with or without OMP-18R5 or OMP-54F28. Data are representative of two independent experiments.

(C) DCs were treated with Wnt5a with or without OMP-18R5 followed by co-culture with naive $CD4^+$ T cells derived from FoxP3-GFP reporter mice. $CD4^+GFP^+$ Tregs were quantified by flow cytometry.

(D) DCs were treated with conditioned media derived from C59-treated versus control-treated BP melanoma cells followed by co-culture with FoxP3-GFP naive $CD4^+$ T cells. $CD4^+GFP^+$ Tregs were quantified by flow cytometry. For (C) and (D), each condition was performed in triplicate. Data are representative of two independent experiments.

(E) Primary tumor growth of syngeneic implanted BP tumors treated with either IgG isotype control, aPD1 alone, OMP-18R5 alone, OMP-54F28 alone, OMP-18R5/aPD1, or OMP-54F28/aPD1 (n = 6/group). All associated data are representative of two independent experiments.

(F) Quantification of lung metastasis in mice related to (E) by H&E microscopy (n = 3/group).

(G) Quantification of tumor-infiltrating $CD8^+$ T cells in mice related to (E) by IHC (n = 3/group).

(H) Flow cytometric analysis of intra-tumoral $CD8^+$ T cells and $CD4^+FoxP3^+$ T cells in mice related to (E).

Data are expressed as $CD8^+$ T cell/$CD4^+FoxP3^+$ T cell ratios. UT, untreated. CM, conditioned media; Ctrl, control. All statistical analyses are based on one-way ANOVA followed by a Tukey post hoc test. All data show mean ± SEM. *$p < 0.05$, **$p < 0.01$, ***$p < 0.001$.

See also Figure S1.

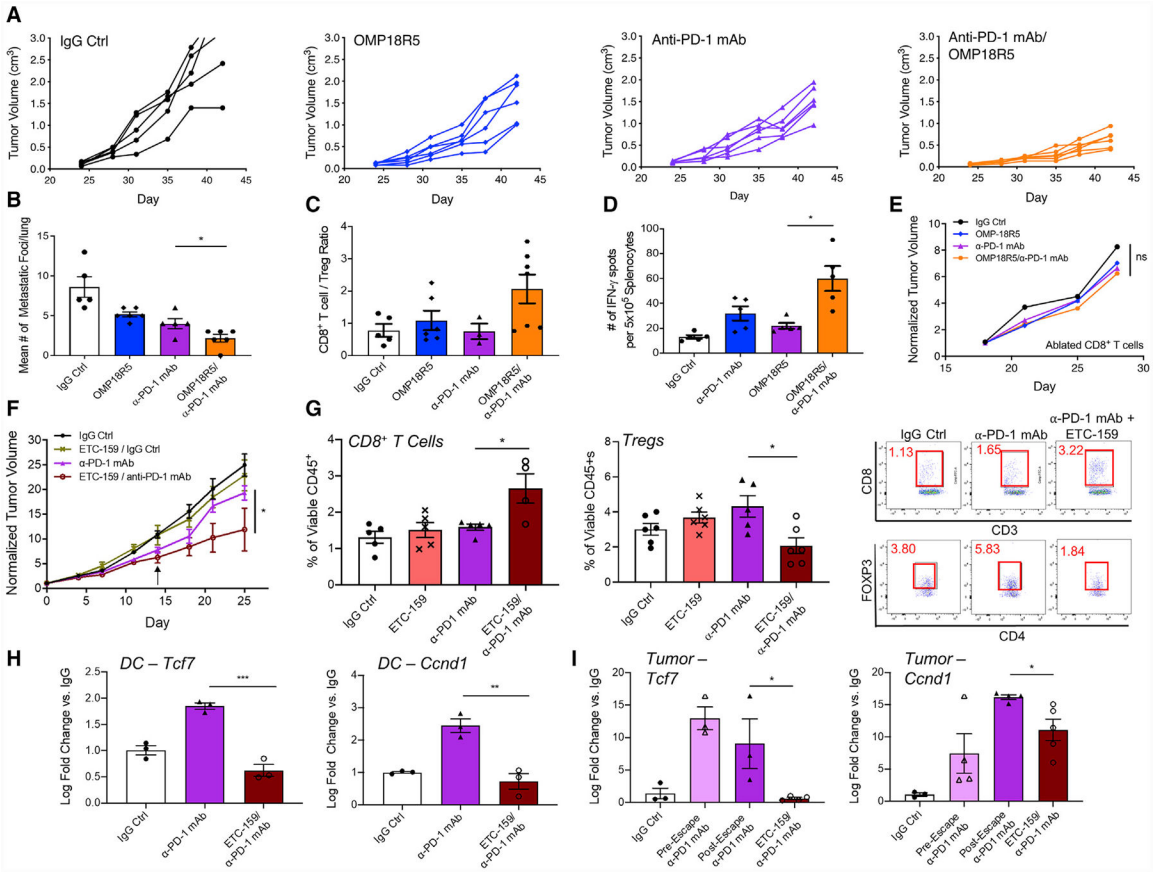

Figure 3. OMP-18R5 and ETC-159 enhance Anti-PD-1 therapy in an autochthonous melanoma model while inhibiting DC b-catenin signaling

(A) Autochthonous BP mice were treated with either IgG isotype ctrl, aPD1, OMP-18R5, or anti-PD-1 + OMP-18R5/aPD1 after the development of primary melanomas (n = 6–7/group). Primary melanoma volumes were recorded every 3 days. All associated data are representative of two independent experiments.

(B) Quantification of lung metastasis in mice related to (A) by H&E microscopy (n = 5/group).

(C) Flow cytometric analysis of intra-tumoral $CD8^+$ T cells and $CD4^+FoxP3^+$ T cells in mice related to (A). Data are expressed as $CD8^+$ T cell/$CD4^+FoxP3^+$ T cell ratios.

(D) Quantification of TRP2-specific $CD8^+$ T cells related to (A) based on IFN-γ ELISpot.

(E) Primary melanoma volumes in autochthonous BP mice treated with anti-CD8 depleting mAb followed by treatment with either IgG isotype ctrl, aPD1, OMP-18R5, or OMP-18R5/aPD1 (n = 5/group).

(F) Autochthonous BP mice were treated with either IgG isotype ctrl, aPD1, delayed ETC-159/IgG ctrl, or delayed ETC-159/aPD1. ETC-159 was initiated at aPD1 escape (black arrow, day 14) (n = 6/group). All associated data are representative of two independent experiments.

(G) Flow cytometric analysis of intra-tumoral $CD8^+$ T cells and Tregs related to (F). (Right) Representative flow dot plots.

(H and I) qRT-PCR analysis of β-catenin target gene expression, *Tcf7* and *Ccnd1*, by tumor-associated DCs (H) or by tumor tissue (I) harvested from mice described in (F) (n = 3/group).

ns, non-significant. Student's two-tailed t test comparing aPD1 monotherapy groups versus combination therapy. All data show mean ± SEM. *p < 0.05, **p < 0.01, ***p < 0.001. See also Figures S2 and S3.

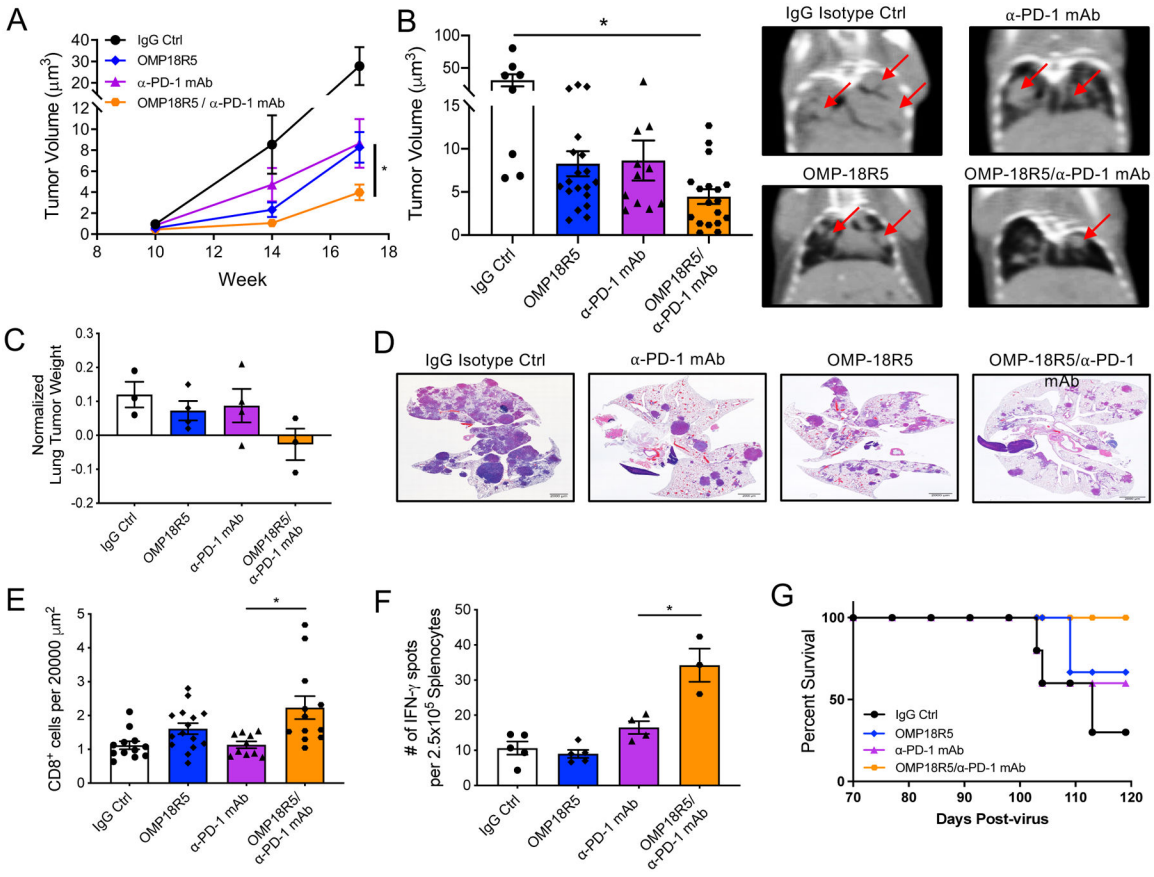

Figure 4. Immunotherapeutic properties of OMP-18R5 extend to an autochthonous model of NSCLC

(A) Cre-expressing adenoviral vector was administered intra-nasally to autochthonous KP mice, inducing primary lung tumor development. At 10 weeks, mice were initiated on IgG ctrl, aPD1, OMP-18R5, or OMP-18R5/aPD1 (n = 6/group). All associated data are representative of two independent experiments.

(B) Micro-CT quantification of tumor volume at weeks 10, 14, and 17 in (A). (Left) Final tumor volumes. Each point represents an individual lung tumor. (Right) Representative images from each treatment group. Red arrows indicate lung tumors. Statistical analyses for (A) and (B) are based on one-way ANOVA followed by a Tukey post hoc test.

(C) Lung weights related to (A). Weights are normalized to lungs harvested from age-matched non-tumor-bearing mice.

(D) Representative H&E sections from each treatment group taken at week 17. Scale bars, 2,000 μm.

(E) IHC quantification of intra-tumoral $CD8^+$ T cells in the experiment described in (A) (n = 5/group).

(F) Quantification of KP cell line-derived antigen-specific splenic $CD8^+$ T cells harvested in (A) based on IFN-γ ELISpot (n = 3–5/group).

(G) Kaplan-Meier survival analysis of mice related to (A). Statistical analysis based on log-rank test, p = 0.06.

A Student's two-tailed t test was performed when comparing aPD1 monotherapy groups versus combination therapy. All data show mean ± SEM. **p < 0.01, *p < 0.05.
See also Figure S4.

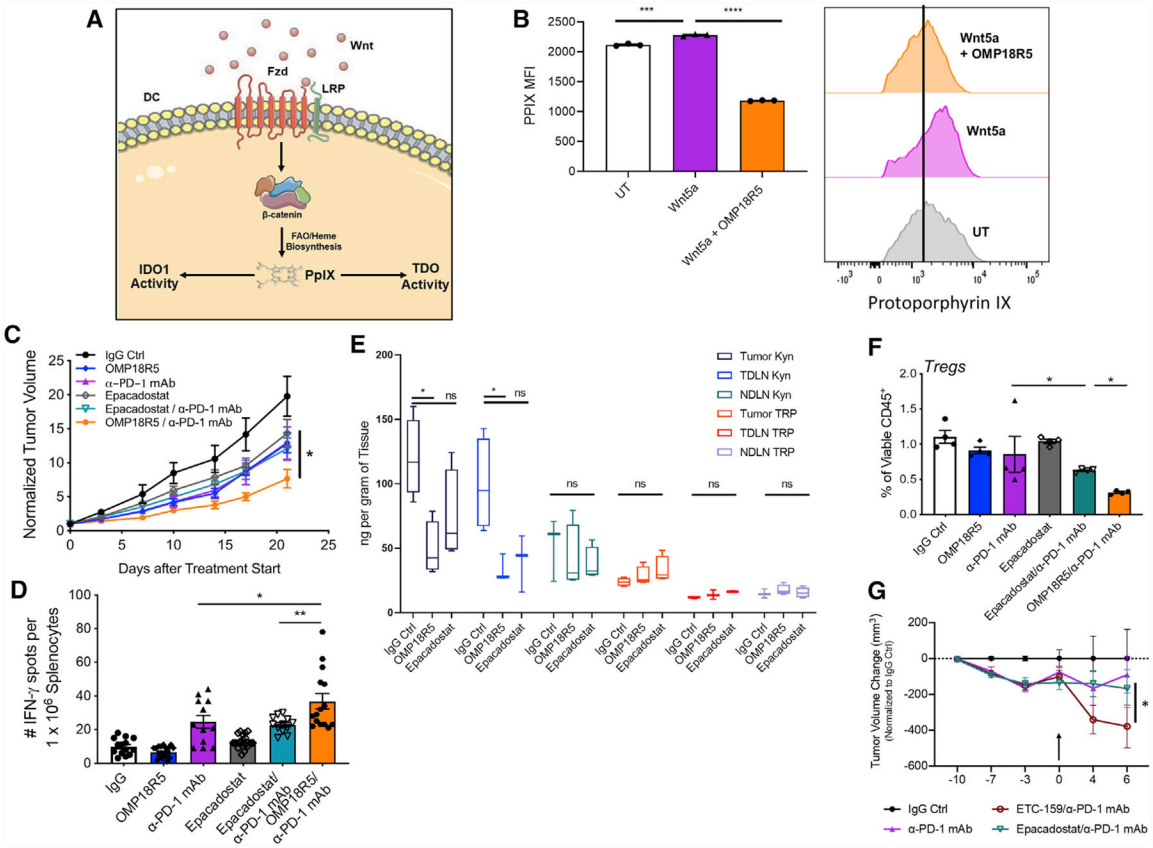

Figure 5. OMP-18R5 suppresses the enzymatic production of kynurenine (Kyn) in the tumor microenvironment and outperforms IDO inhibition in vivo

(A) Schematic representation of Wnt ligand-driven DC fatty-acid oxidation (FAO)/heme biosynthesis, resulting in protoporphyrin IX (PpIX) generation and tryptophan (Trp)-degrading enzymatic activity.

(B) DCs treated with Wnt5a with or without OMP-18R5 prior to incubation with aminolevulinic acid (ALA) and flow cytometric quantification of PpIX levels. Performed in triplicate. (Right) Representative PpIX flow histogram. Data are representative of three independent experiments.

(C) Autochthonous BP mice were treated with either IgG isotype ctrl, aPD1, OMP-18R5, epacadostat, OMP-18R5/aPD1, or epacadostat/aPD1 after the development of primary melanomas (n = 9–11/group).

(D) Quantification of TRP2-specific $CD8^+$ T cells derived from (C) based on IFN-γ ELISpot.

(E) LC-MS/MS analysis of Kyn and Trp from tumor, TDLNs, and non-tumor draining LN (NDLN) tissues following treatment with either OMP-18R5 or epacadostat (n = 4/group). Data are representative of two independent experiments.

(F) Flow cytometric analysis of intra-tumoral Tregs derived from tumor tissues harvested from (C) (n = 4/group). Data are representative of two independent experiments.

(G) Autochthonous BP mice were treated with either IgG isotype ctrl, aPD1, delayed ETC-159/aPD1, or delayed epacadostat/aPD1 where ETC-159 and epacadostat were initiated at aPD1 escape (black arrow, day 0) (n = 6/group).

Tumor volumes were normalized to IgG isotype control group. All statistical analyses were based on one-way ANOVA followed by a Tukey post hoc test. All data show mean ± SEM. *$p < 0.05$, **$p < 0.01$, ***$p < 0.001$, ****$p < 0.0001$.
See also Figure S5.

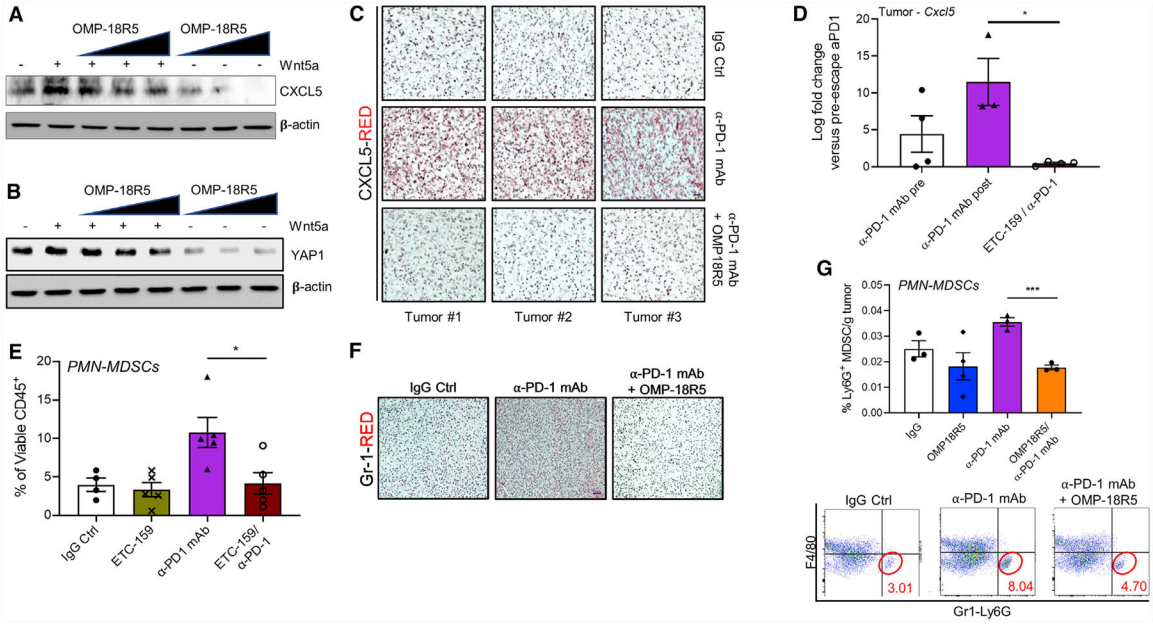

Figure 6. Wnt ligand inhibition suppresses PMN-MDSC influx into tumors

(A and B) CXCL5 (A) and (B) YAP1 western blot analysis of the BP melanoma cell line treated with Wnt5a with or without OMP-18R5. Data are representative of three independent experiments.

(C) CXCL5 IHC of resected BP melanoma tissues following treatment with IgG control, aPD1, or OMP-18R5/aPD1. Data are representative of two independent experiments. Scale bar, 20 μm.

(D) qRT-PCR analysis of *Cxcl5* expression levels in autochthonous BP melanomas before aPD1 escape, following aPD1 escape, and after delayed treatment with ETC-159 (dETC-159) (n = 3/group). Data are representative of two independent experiments.

(E) Flow cytometry analysis of intra-tumoral $CD11b^{+}Ly6G^{+}Ly6C^{lo}F4/80^{-}$ PMN-MDSCs normalized by tumor size. Data are representative of two independent experiments.

(F) Gr-1 IHC analysis of autochthonous BP melanoma tumors treated with IgG control, aPD1, or OMP-18R5/aPD1. Data are representative of three independent experiments. Scale bar, 50 μm.

(G) Flow cytometry analysis of intra-tumoral $CD11b^{+}Ly6G^{+}Ly6C^{lo}F4/80^{-}$ PMN-MDSCs/g of tumor in the LLC model following treatment with IgG control, aPD1, or OMP-18R5/ aPD1 (n = 3/group). (Below) Representative flow dot plots.

Data are representative of two independent experiments. A Student's two-tailed t test was used to compare aPD1 monotherapy groups versus combination therapy. All data show mean ± SEM. *$p < 0.05$, ***$p < 0.001$.

See also Figures S6A and S6B.

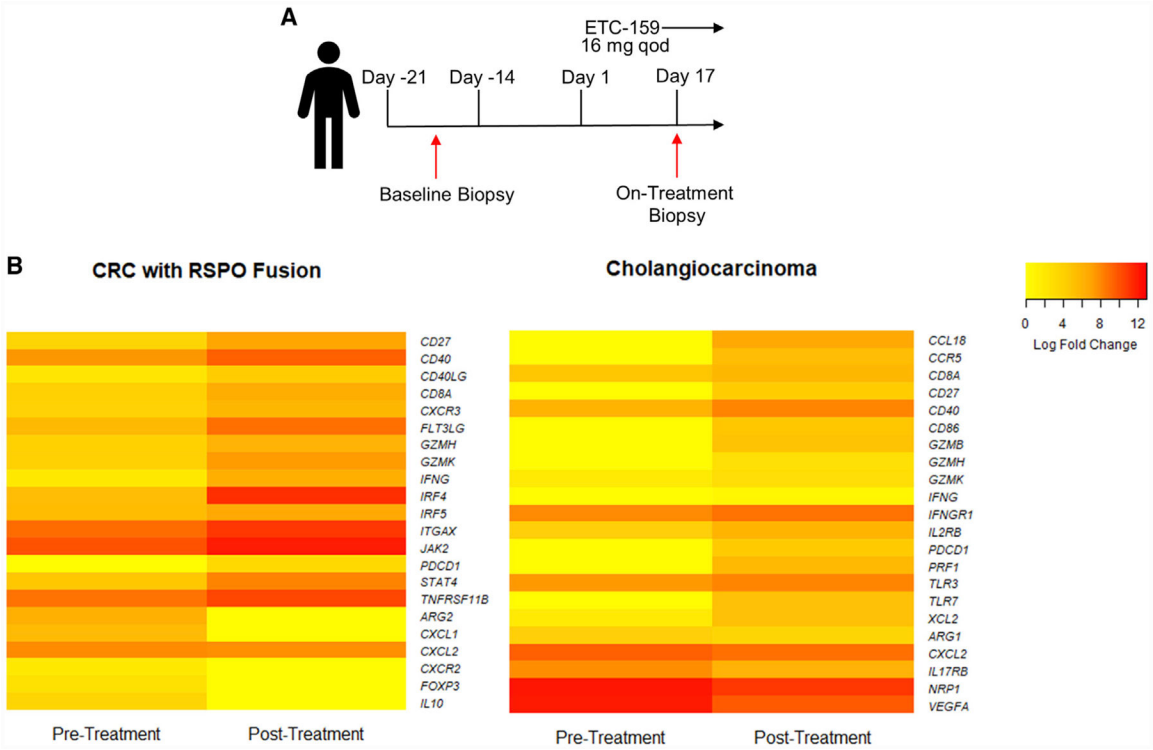

Figure 7. Wnt ligand inhibition with ETC-159 promotes the development of a more favorable tumor immune microenvironment in patients

(A) Schematic of patient tumor biopsies prior to and following exposure to ETC-159.

(B) NanoString analysis of immune-related gene expression. Heatmaps illustrate log fold change in gene expression between pre- and post-treatment tumor specimens derived from two cancer patients.

See also Figure S6C and Tables S3 and S4.

KEY RESOURCES TABLE

REAGENT or RESOURCE	SOURCE	IDENTIFIER
Antibodies		
Anti-mouse CD45, PerCp-Cy5.5 conjugated, clone:30-F11	BD PharMingen	Cat# 550994; RRID:AB_394003
Anti-mouse CD3e, FITC conjugated, clone: 145–2C11	BD PharMingen	Cat# 553061; RRID:AB_394594
Anti-mouse CD8a, BV510 conjugated, clone: 53-6.7	BD PharMingen	Cat# 563068; RRID:AB_2687548
Anti-mouse CD4, APC conjugated, clone: RM4-5	BD PharMingen	Cat# 553051; RRID:AB_398528
Anti-mouse Foxp3, PE conjugated, clone: MF23	BD PharMingen	Cat# 560408; RRID:AB_1645251
Anti-mouse CD11b, PE conjugated, clone: M1/70	BD PharMingen	Cat# 557397; RRID:AB_396680
Anti-mouse F4/80, APC conjugated, clone: BM8	BioLegend	Cat # 123116; RRID:AB_893481
Anti-mouse Ly-6G, FITC conjugated, clone: 1A8	BD PharMingen	Cat# 551460; RRID:AB_394207
Anti-mouse CD16/CD32 (Fc block), clone: 2.4G2	BD PharMingen	Cat # 553142; RRID: AB_394657
Anti-mouse CD3e, PerCP-Cy5.5 conjugated, clone: 145–2C11	BD PharMingen	Cat# 551163; RRID:AB_394082
Anti-mouse CD8a, FITC conjugated, clone: 53-6.7	BD PharMingen	Cat# 553031; RRID:AB_394569
Anti-mouse CD4, FITC conjugated, clone: RM4-5	BD PharMingen	Cat# 553047; RRID:AB_394583
Anti-mouse CD11c, PE conjugated, clone: HL3	BD PharMingen	Cat# 553802; RRID:AB_395061
Anti-mouse CD103, BV421 conjugated, clone: M290	BD PharMingen	Cat # 562771; RRID: AB_2737783
Anti-mouse F4/80, FITC conjugated, clone: BM8	BioLegend	Cat # 123108; RRID: AB_893502
Anti-mouse B220, FITC conjugated, clone: RA3–6B2	BioLegend	Cat # 103206; RRID: AB_312991
Anti-mouse I-A/I-E (MHCII) Antibody, PE-Cy7 conjugated, clone: M5/114.15.2	BioLegend	Cat # 107628; RRID: AB_2069377
Anti-mouse CD8a, APC conjugated, clone: 53-6.7	BD PharMingen	Cat# 553035; RRID: AB_398527
Rabbit anti-mouse CD8a, clone: D4W2Z	Cell Signaling Technologies	Cat# 98941; RRID:AB_2756376
Anti-mouse CXCL5	LsBio	Cat # LS-C104413; RRID AB_10624103
Rat anti-mouse Ly6G	Abcam	Cat# ab25377; RRID:AB_470492
Rat anti-moue IDO1, clone: mIDO-48	Santa Cruz Biotechnology	Cat# sc-53978; RRID:AB_831071
Rabbit anti-TDO2	Proteintech	Cat# 15880–1-AP; RRID:AB_2827610
Rabbit anti-mouse β-Catenin, clone: D10A8	Cell Signaling Technologies	Cat# 8480; RRID:AB_11127855
Anti-mouse CD45, PerCp-Cy5.5 conjugated, clone:30-F11	BD PharMingen	Cat# 550994; RRID:AB_394003
Anti-mouse CD3e, FITC conjugated, clone: 145–2C11	BD PharMingen	Cat# 553061; RRID:AB_394594
Anti-mouse CD8a, BV510 conjugated, clone: 53-6.7	BD PharMingen	Cat# 563068; RRID:AB_2687548
OMP-18R5	OncoMed	N/A
OMP-54F28	OncoMed	N/A
Anti-PD-1, clone: RMP-14	BioXCell	Cat# BE0146; RRID:AB_10949053
Anti-CD8	Duke Cell Culture Facility	N/A
Rat IgG2a isotype control, clone: 2A3	BioXCell	Cat# BE0089; RRID: AB_1107769
Bacterial and virus strains		
Ad5CMVCre	Univ. of Iowa	Cat # Ad5CMVCre
Biological Samples		

REAGENT or RESOURCE	SOURCE	IDENTIFIER
Human melanoma tissue specimens	Duke University Hospital	N/A
Pre and Post ETC-159 treated human tumor specimens	A*STAR	N/A
Chemicals, peptides, and recombinant proteins		
Collagenase IV	Sigma-Aldrich	Cat # C-5138
Hyaluronidase	Sigma-Aldrich	Cat # H-6254
DNaseI	Sigma-Aldrich	Cat # D-5025
RPMI	Sigma-Aldrich	Cat # R8758
RBC Lysis Buffer	Sigma-Aldrich	Cat # R7757
Live/Dead Fixable Violet Dead Cell Stain Kit	ThermoFisher	Cat # L34955
Live/Dead Fixable Aqua Dead Cell Stain Kit	ThermoFisher	Cat # L34966
Recombinant Wnt5a	R&D systems	Cat # 645-WN-010
Aminolevulenic acid	Sigma	Cat # A3785
Hematoxylin	VWR	Cat # 95057–844
Eosin	VWR	Cat # 95057–848
Vina Green Chromogen Kit	BioCare Medical	Cat # BRR 807 AH
Warp Red Chromogen Kit	BioCare Medical	Cat # 901-WR806–081017
NP40 lysis buffer	Sigma-Aldrich	Cat #492016
RIPA Lysis and Extraction Buffer	ThermoFisher	Cat # 89901
Protease Inhibitor Cocktail	Roche	Cat #4693159001
PhosSTOP	Roche	Cat # 4906845001
$TRP2_{180–188}$ peptide	ANASPEC	Cat # AS-61058
$MUT1_{51–58}$ peptide	BACHEM	Cat # 4026648
$OVA_{257–264}$ peptide	InvivoGen	Cat # vac-sin
C-59	Selleckchem	Cat # S7037
ETC-159	A*STAR	N/A
Collagenase IV	Sigma-Aldrich	Cat # C-5138
Recombinant Mouse IL-4	BioAbChem	Cat # 42-IL4
Recombinant Mouse GM-CSF	R&D System	Cat # 415-ML-010
4-hydroxytamoxifen	Sigma-Aldrich	Cat # H6278–10MG
Polyethyelene glycol(PEG)-8000	Sigma-Aldrich	Cat # 89510–250G-F
Critical commercial assays		
Mouse Kynurenine ELISA kit	MyBioSource	Cat # MBS043489
Mouse IFNγ ELISPOT Plus	Mabtech	Cat # 3321-4APT-2
Mouse FoxP3 Buffer Set	BD Biosciences	Cat # 560409
Miltenyi CD11c magnetic selection columns	Miltenyi Biotec	Cat # 130-108-338
Naive $CD4^+$ T cells selection kit	Stem Cell Technologies	Cat # 19765
RNAeasy Plus Micro kit	QIAGEN	Cat # 74034
SuperScript IV FirstStrand Synthesis System	Invitrogen	Cat # 11756050
PowerUp Master Mix	Applied Biosciences	Cat # A25742
Deposited data		

REAGENT or RESOURCE	SOURCE	IDENTIFIER
RNA-seq data derived from the murine $BRAF^{V600E}PTEN^{-/-}$ melanoma anti-PD-1 resistance study	Hanks Lab; Theivanthiran et al., 2020; Zhao et al., 2018a	SAMN09878780
RNA-seq dataset derived from metastatic melanoma patients prior to anti-PD-1 treatment	Hugo et al., 2016	GEO: GSE78220
Wnt pathway-focused Nanostring dataset derived from metastatic melanoma patients prior to anti-PD-1 treatment	This paper	GEO: GSE165745
Nanostring data from ETC-159 treated patients	This paper	GEO: GSE167039
Experimental models: Cell lines		
$Braf^{V600E}Pten^{-/-}$ (BPD6, male) cell line	Hanks Lab	N/A
$p53^{flox/flox}$;$Kras^{G12D}$ cell line	Hanks Lab	N/A
Lewis Lung Carcinoma	ATCC	ATCC Cat# CRL-1642; RRID:CVCL_4358
DC2.4	Kenneth Rock, University of Massachusetts Medical School	Shen et al., 1997; RRID: CVCL_J409
HEK293-LEF1/TCF-luciferase cell line	N/A	Ring et al., 2011
Experimental models: Organisms/strains		
B6.CgBRAF^{tm1Mmcm}PTEN^{tm1Hwu}Tg(TyrCre/ERT2)13Bos/BosJ ($BRAF^{V600E}$ $PTEN^{-/-}$, H-2^{b}) transgenic mice	Jackson Labs	IMSR Cat# JAX:013590; RRID:IMSR_JAX:013590
$p53^{flox/flox}$;$Kras^{G12D}$ transgenic mice	Anton Berns, Netherlands Cancer Institute	DuPage et al., 2009
C57BL/6 wild type	Jackson Labs	IMSR Cat# JAX_000664; RRID:IMSR_JAX:000664
BALB/c (H-2^{d}) wild type	Jackson Labs	IMSR Cat# JAX_000651; RRID:IMSR_JAX:000651
B6.Cg-Foxp3^{tm2Tch}/J (FoxP-EGFP, H-2^{b})	Jackson Labs	IMSR Cat# JAX:006772; RRID:IMSR_JAX:006772
B6.CgBRAF^{tm1Mmcm}PTEN^{tm1Hwu}Tg(TyrCre/ERT2)13Bos/BosJ ($BRAF^{V600E}$ $PTEN^{-/-}$, H-2^{b}) transgenic mice	Jackson Labs	IMSR Cat# JAX:013590; RRID:IMSR_JAX:013590
Oligonucleotides		
Tcf7-forward: AGC TTT CTC CAC TCT ACG AAC A	IDT	N/A
Tcf7-reverse: AAT CCA GAG AGA TCG GGG GTC	IDT	N/A
Ccnd1-forward: GCG TAC CCT GAC ACC AAT CTC	IDT	N/A
Ccnd1-reverse: CTC CTC TTC GCA CTT CTG CTC	IDT	N/A
Gapdh-forward: GTC TAC ATG TTC CAG TAT GAC TCC	IDT	N/A
Gapdh-reverse: AGT GAG TTG TCA TAT TTC TCG TGG T	IDT	N/A
Cxcl2-forward: GAG CTT GAG TGT GAC GCC CCC AGG	IDT	N/A
Cxcl2-reverse: GTT AGC CTT GCC TTT GTT CAG TATC	IDT	N/A
Cxcl5-forward: GCA TTT CTG TTG CTG TTC ACG CTG	IDT	N/A
Cxcl5-reverse: CCT CCT TCT GGT TTT TCA GTT TAG C	IDT	N/A
Actb-forward: GTC TAC ATG TTC CAG TAT GAC TCC	IDT	N/A
Actb-reverse: AGT GAG TTG TCA TAT TTC TCG TGG T	IDT	N/A
Ccl4-forward: GCC CTC TCT CTC CTC TTG CT	IDT	N/A
Ccl4-reverse: GTC TGC CTC TTT TGG TCA GG	IDT	N/A
Software and algorithms		

REAGENT or RESOURCE	SOURCE	IDENTIFIER
nSolver	Nanostring	RRID: SCR_003420
Amira 3D Visualization and Analysis Software Suite	FEI, Thermo Fisher Scientific	RRID: SCR_007353
ImageJ	ImageJ	RRID: SCR_003070
FlowJo Version 10	Tristar	RRID: SCR_008520
Prism	GraphPad	RRID: SCR_002798
ImmunoCapture and ImmunSpot	ImmunoSpot	RRID: SCR_011082
R	R Project for Statistical Computing	RRID:SCR_001905
Heatmap.2	R Function	https://cran.r-project.org/web/packages/gplots/index.html
Other		
XRAD225 Cx	Precision X-Ray, Inc	N/A
gentleMACS Tissue Dissociator	Miltenyi Biotec	Cat # 130-093-235
FACSCanto II	Becton Dickinson	N/A
LSRII	Becton Dickinson	N/A
gentleMACS C-tubes	Miltenyi Biotec	Cat # 130-093-237
gentleMACS M-tubes	Miltenyi Biotec	Cat # 130-093-236